Age-dependent Shift in the de Novo Proteome Accompanies Pathogenesis in an Alzheimer's Disease Mouse Model

Megan Elder
New York University
Hediye Erdjument-Bromage
New York University School of Medicine
Mauricio Oliveira
New York University
Maggie Mamcarz
New York University
Thomas Neubert
New York University School of Medicine
Eric Klann (eklann@cns.nyu.edu)
New York University https://orcid.org/0000-0001-7379-6802

Article

Keywords: Alzheimer's disease, neurodegenerative disorder, molecular abnormalities, protein synthesis

Posted Date: September 22nd, 2020

DOI: https://doi.org/10.21203/rs.3.rs-67262/v1

Version of Record: A version of this preprint was published at Communications Biology on June 30th, 2021. See the published version at https://doi.org/10.1038/s42003-021-02324-6.

Age-dependent shift in the *de novo* proteome accompanies pathogenesis in an Alzheimer's disease mouse model

Megan K. Elder[1], Hediye Erdjument-Bromage[2,3], Mauricio M. Oliveira[1], Maggie Mamcarz[1], Thomas A. Neubert[2,3], Eric Klann[1*]

1. Center for Neural Science, New York University, New York, NY 10003, USA
2. Department of Cell Biology, New York University School of Medicine, New York, NY 10016, USA
3. Kimmel Center for Biology and Medicine at the Skirball Institute, New York University School of Medicine, New York, NY 10016, USA

*Correspondence should be addressed to Eric Klann at ek65@nyu.edu

Abstract

Alzheimer's disease (AD) is an age-related neurodegenerative disorder, however neuropathological changes begin years before memory impairment. Investigation of the early molecular abnormalities in AD might offer innovative opportunities to target memory impairment prior to onset. Decreased protein synthesis plays a fundamental role in AD, yet the consequences of this dysregulation for cellular function remain unknown. We hypothesize that alterations in the *de novo* proteome drive early metabolic alterations in the hippocampus that persist throughout AD progression. Using a combinatorial amino acid tagging approach to selectively label and enrich newly synthesized proteins, we found that the *de novo* proteome is disturbed in young APP/PS1 mice prior to symptom onset, affecting the synthesis of multiple components of the synaptic, lysosomal and mitochondrial pathways. Furthermore, the synthesis of large clusters of ribosomal subunits were affected throughout development. Our data suggest that large-scale changes in protein synthesis could underlie cellular dysfunction in AD.

Introduction

Alzheimer's disease (AD) is an age-related neurodegenerative condition characterized by progressive and devastating cognitive impairment. AD is classically characterized by extensive deposition of amyloid beta (Aβ) plaques and intracellular inclusions of hyperphosphorylated tau, in the form of neurofibrillary tangles[1]. In addition to the deposition of plaques and tangles, AD is also characterized by extensive atrophy of the brain, which follows a prescribed trajectory throughout disease progression. Initially atrophy is restricted to the hippocampi and medial temporal lobes, even before the

appearance of symptoms[2]. The cause of this neuronal atrophy has not yet been elucidated, but it is likely that pathological alterations in protein synthesis are a contributing factor[3]. In a healthy biological system, proteins are made and degraded in a controlled process termed protein homeostasis (proteostasis). However, the intrinsic and extrinsic stressors that accumulate with age and disease can challenge the delicate balance between protein synthesis and degradation[4].

Removal of misfolded or otherwise damaged proteins is essential to avoid toxicity and is regulated by a variety of proteolytic systems, whose dysfunction has been implicated in AD pathophysiology[5]. Proteasomal activity is perturbed in vulnerable cortical areas and the hippocampus in late stage AD[6], whereas proteolysis has been shown to be impaired in very mild stages of the disease, suggesting that proteostasis disruption might occur prior to the development of symptoms[7].

On the opposite side of the proteostatic balance is protein synthesis. Following transcription, mRNA is translated to a polypeptide chain via ribosomal activity, a process that in neurons occurs both somatically and locally in projections[8]. This *de novo* protein synthesis is a dynamic process, as it is necessary for basal neuronal function, responding to stimuli that induce long-lasting plasticity, and for memory consolidation[9,10]. In AD, multiple studies have observed dysregulation of translation throughout the disease process, as indicated by changes in p70 S6 kinase 1, eukaryotic initiation factors 2 alpha (eIF2α) and 4E (eIF4E) phosphorylation[11-16], as well as decreased ribosomal function[3,17-19]. Curiously, altered expression of ribosomal RNAs and ribosomal protein-coding mRNAs in the hippocampus appear even prior to the onset of symptoms and the development of hallmark AD pathologies[3,17]. Furthermore, ribosomal dysfunction is

specific to cortical areas that show the greatest atrophy in later stages of the disease, including the inferior parietal lobule and superior middle temporal gyri[17].

Although alterations in the level of *de novo* protein synthesis in AD have been implied for several years, the mechanistic details involved in this dysregulation remain largely unknown[20]. When monitored in APP/PS1 mutant mice, which express familial AD-associated mutations in the amyloid precursor protein (APP_{swe}) and presenilin-1 genes ($PS1_{\Delta E9}$)[15], an approximately 30% decrease in *de novo* protein synthesis was observed in aged, symptomatic APP/PS1 mice compared to wild-type littermates[15]. Elucidating the identity of these dysregulated proteins has become an important focus of research, and two independent studies of transgenic mice that experimentally model different aspects of AD pathology have used *in vivo* metabolic labelling to isolate *de novo* synthesized proteins for subsequent mass spectrometry analysis[21,22]. The use of a less complex system, such as isolated hippocampal slices, offers a different resolution and a narrower timeframe for this snapshot of the *de novo* proteome.

Herein, we used BONLAC, a combinatorial approach of stable isotope labelling by amino acid tagging (SILAC) and biorthogonal noncanonical amino acid tagging (BONCAT), and mass spectrometry to compare *de novo* protein synthesis in acute hippocampal slices from 4-month-old and 12-month-old APP/PS1 mutant mice for the identification and measurement of relative abundance of *de novo* synthesized proteins[21,23-28]. Here, we show for the first time a significant dysregulation of proteostasis even before symptom onset in 4-month-old mice, with significant alterations in networks of proteins involved in both protein degradation and synthesis. Further, in aged APP/PS1 mice that display memory impairments[29], we observed dysregulation of both lysosomal

and mitochondrial proteins, as well as components of the ribosome. Together, these findings suggest that alterations in the synthesis of proteins involved in a variety of critical cellular pathways are impaired early in the AD process and likely underlie the deterioration of neuronal function, leading to loss of memory.

Results

Aging-related downregulation of hippocampal protein synthesis in APP/PS1 mutant mice

Previous studies using puromycin and azidohomoalanine (AHA) incorporation to label newly synthesized proteins in mice modeling aspects of AD pathology demonstrated a reduction in *de novo* protein synthesis[15,21,22,30], and the translation efficiency of polyribosomes isolated from the mild cognitive impairment (MCI) and end-stage AD brain is reduced by >60% in affected cortical areas[17]. We first confirmed that histopathological changes are observed in the brain of 4 vs 12 month-old APP/PS1 mice by performing immunohistochemistry against Aβ in brain sections including the dorsal hippocampus. As expected, we found that the amyloid deposits are severely increased in the brains of aged APP/PS1 mice when compared to younger APP/PS1 mice (Figure 1a-c). Using BONCAT labeling, we observed a ~20% decrease in the level of *de novo* protein synthesis in 12 month-old APP/PS1 mice compared to 4 month-old APP/PS1 mice (Figure 1d). Collectively, these findings support and extend previous work conducted in our laboratory, which highlighted a significant decrease in *de novo* protein synthesis between aged WT and APP/PS1 mice using SUnSET, another non-radioactive method for tagging and monitoring new protein synthesis[15]. Therefore, using BONLAC labeling we proceeded to

identify changes in the *de novo* proteome in the young and aged APP/PS1 mutant mice (Figure 1e).

Large-scale proteomic dysfunction is observed early in the hippocampus of APP/PS1 mice

In order to identify candidate proteins of interest, we used BONLAC and a previously published multi-layered analysis based in coincidence detection[23,28]. In the hippocampi of 3-5 month-old mice, 2510 *de novo* synthesized proteins were measured in at least one sample. 1826 proteins were measured across the majority of samples (Supplementary Figure 1), and of these 1826, 180 were differentially regulated in the APP/PS1 mice (Figure 2a; Supplementary Figure 2). The majority of differentially regulated proteins were upregulated (fold change ≥ 1.2; 107 or 5.9% of total proteins), whereas 73 proteins were downregulated (fold change ≤ 0.8; 4.0% of total proteins; Figure 2b) in the APP/PS1 mice. When the biological relevance of these changes were interrogated using DAVID and StringDB, the GO and KEGG pathways that were highlighted included the cellular component ‘postsynapse’, as well as proteostasis-related components, gathered under the terms ‘proteasome’ and ‘ribosome’ (Figure 2c-d). These findings indicate that even in young APP/PS1 mice that do not show memory deficits, processes that are both previously linked to AD, and are critical to cell functioning are disturbed.

Alterations in the *de novo* proteome correspond with pathologies in aged APP/PS1 mice

Following these investigations in young APP/PS1 mice, we investigated the impact of aging and the development of AD-like pathology on the *de novo* proteome. As expected

from the decreased rate of translation apparent in AHA incorporation levels (Figure 1d), fewer newly synthesized proteins were observed in APP/PS1 mice aged ≥ 12 months compared to younger mice. In the hippocampi of these aged mice, 2065 proteins were measured at least once (Supplementary Figure 3), 855 proteins were measured across the majority of samples, and 113 proteins were consistently altered in the APP/PS1 mice (Figure 3a; Supplementary Figure 4). Proteins whose synthesis was reduced by 20% compared to age-matched WT mice made up 2.7% of the consistently detected proteins (23 proteins), while BONLAC detected 90 proteins with increased *de novo* synthesis in the APP/PS1 mice (10.6%; Figure 3b). Through GO analysis via DAVID and visualization using StringDB, we observed several functional clusters (Figure 3c), with the top hits including 'Alzheimer's disease', 'ribosome', and 'lysosome' (Figure 3d). Together, these findings indicate that the dysregulation of core cellular processes relies at least partially on impaired protein synthesis, and that changes in *de novo* proteome happen even before full pathology onset.

Dysregulation of the synthesis of BONLAC-identified candidates is reflected in protein expression

Next, to understand whether these changes in *de novo* protein synthesis corresponded to altered protein expression, we validated candidates from several enriched clusters using western blotting, comparing changes in expression between APP/PS1 and wild-type littermates. Aiming to validate differences from the same group used for proteomic studies, we reserved BONLAC-labeled acute hippocampal slices from animals prior to sample preparation for mass spectrometry analysis, and instead lysed the tissue for gel

electrophoresis (Figure 4a). Alongside APP, which was selected as a positive control[31], other AD-associated proteins known to be involved in lysosome-mediated protein degradation (cathepsin-d; ctsd[32,33]) and synaptic plasticity (neuromodulin; GAP-43[34,35]) were probed. Samples were also probed for the expression of the large 60S ribosomal proteins Rpl13 and Rpl18. As shown in Figure 4b and Figure 4c, the *de novo* synthesis and the total expression of APP were increased in both age groups of APP/PS1 mice, as expected. Neither the synthesis nor the expression of Ctsd protein were altered in young APP/PS1 mice compared to wild-type littermates. However in aged, symptomatic mice, a similar trend was found in both BONLAC and total protein levels. In contrast to younger mice, the older APP/PS1 mice also showed significantly reduced synthesis and total expression of the synaptic protein GAP-43, which corresponds with a known decline in synaptic density at this age[36].

The large 60S ribosomal subunit protein Rpl13 also was profiled after BONLAC labelling indicated hippocampal synthesis of this protein was decreased in APP/PS1 mutant mice throughout aging. Western blot analysis confirmed that there was a reduction in expression of this ribosomal protein in both groups of APP/PS1 mice, however no statistically significant differences were observed. The expression of an additional ribosomal protein, Rpl18, was investigated as BONLAC labelling indicated the synthesis of this protein varied throughout the development of pathology in the APP/PS1 mice. In young mice, both newly synthesized and total expression of Rpl18 were decreased relative to wild-type mice, whereas both measures were increased in older APP/PS1 mice, although no significance was determined. Next, we performed a linear regression analysis between the BONLAC and western blot fold changes (APP/PS1 vs. WT) to

evaluate whether a linearity existed between the values. Linear regression analysis highlighted a significant correlation between detection of the candidate protein in the *de novo* analysis vs. candidate protein expression in the total protein fraction (Figure 4d). Together, these results indicate that altered synthesis of proteins detected with BONLAC are correlated with changes in global protein expression.

Cluster analysis of commonly synthesized proteins in both young and aged APP/PS1 mice highlights key AD pathways

Following the corroboration of BONLAC candidates by western blotting, we further investigated the overall patterns of protein synthesis regulation observed in the APP/PS1 mice. Although examination of significant changes (as detected by C-score analysis) reveal statistically relevant alteration of the *de novo* proteome, it is noteworthy that smaller fluctuations in expression (fold change < 20%: labelling ratio > 0.8 or < 1.2) can also provide information as to whether a specific cell process is altered. Therefore, we compared all 791 newly synthesized proteins identified in both 3-5 month-old and 12+ month-old APP/PS1 mice and their wild-type littermates. To investigate whether any biological pathways were differentially affected, we conducted hierarchical clustering analysis using Cytoscape. Several key clusters were observed (Figure 5, Supplementary Table 1), closely associated with the KEGG pathways ‘Alzheimer’s disease’ (Figure 5 Cluster 5; Supplementary Figure 9) and ‘protein processing in the endoplasmic reticulum’ (Figure 5 Cluster 1; Supplementary Figure 5). The GO terms ‘synapse’ (Figure 5 Cluster 2; Supplementary Figure 6), and ‘synaptic vesicle cycle (Figure 5 Cluster 3; Supplementary Figure 7) were enriched in this analysis, as were the GO terms ‘axo-

dendritic transport' (Figure 5 Cluster 4; Supplementary Figure 8), 'myelin sheath' (Figure 5 Cluster 5; Supplementary Figure 9), 'mitochondrial part' and 'electron transfer activity' (Figure 5 Cluster 6; Supplementary Figure 10).

Dysregulation of ribosomal protein synthesis is a common feature in APP/PS1 mice throughout the aging process

As described above, C-score detection of candidates generated a list of proteins that were highly dysregulated in the APP/PS1 hippocampus (+/- 20% compared to wild-type). When these dysregulated candidate proteins were compared between age groups, only 31 proteins were significantly dysregulated in both the young and aged APP/PS1 mice relative to age-matched WT littermates (Figure 6a). The majority of these proteins showed either an increased level of synthesis at both ages (11/31) or reversed expression (decreased synthesis in young APP/PS1 mice and increased synthesis in aged mice, or vice versa; 15/31) in comparison to wild-type mice. Only five proteins showed consistently decreased synthesis in the APP/PS1 mice, regardless of age (Figure 6b). Identification of the proteins consistently dysregulated in the APP/PS1 mice highlighted a significant cluster of ribosomal proteins, three of which are components of the small 40S ribosomal subunit, and six of which are components of the large 60S ribosomal subunit (Figure 6c). Taken as a whole, these results support the notion that alterations in the expression of ribosomal proteins is an early feature of AD pathology, and may well play a role in protein synthesis dysfunction through the course of disease.

Discussion

Dysregulated proteostasis underlies many of the hallmark pathologies of AD. Both the deposition of Aβ in the form of plaques and accumulation of hyperphosphorylated tau-containing tangles suggest impaired protein degradation systems, and indeed, dysfunctional proteolysis has been observed in AD brains[5]. Further, translation is impaired throughout the AD process[10-17] and *de novo* protein synthesis is decreased in mouse lines that model various aspects of AD pathology[15,21,22]. The identity of the proteins which are differentially synthesized before and after AD symptom onset in the human brain are unknown. Interestingly however, ribosomal function was shown to be impaired in the brains of individuals diagnosed with mild cognitive impairment[17].

Recently, the *de novo* proteome of mouse lines that model aspects of AD have become a focus of study. Decreased *de novo* protein synthesis was observed in neurons with high levels of hyperphosphorylated tau in the K369I (K3) and rTg4510 transgenic mouse models of tauopathy and neurodegeneration[21]. Moreover, and consistent with our findings, investigation using *in vivo* metabolic labelling has highlighted significant dysregulation of the synthesis of proteins involved in vesicle transportation and mitochondrial functioning prior to symptom onset in APP/PS1 mice[22]. This study also investigated changes in the proteome both pre- and post-symptom onset, but the young, asymptomatic mice selected for the study (2 months-old) do not yet show hallmark Aβ deposition in the hippocampus, which begins at 3-4 months of age[31]. Further, although no memory deficits are observed by this age, alterations in neuronal excitability in the hippocampus have previously been reported in 4 month-old APP/PS1 mice[37]. Moreover, although significant impairments in hippocampal LTP and cognitive ability are apparent by 9 months of age[31,38,39], the age selected for the symptomatic group in this work, several

studies have indicated that older mice (>12 months old) possess greater deficits in spatial learning and memory[40-43].

In the present study, we used BONLAC labelling in acute hippocampal slices from ~4 month-old and ~12 month-old symptomatic APP/PS1 mice and their wild-type littermates to isolate and identify alterations in the *de novo* hippocampal proteome. The use of animals at these ages both supports the recent *in vivo* work described above[22], and extends the coverage of the *de novo* proteome investigations throughout pathology development in this model. Decreased synthesis was observed in aged APP/PS1 mice, as represented by lower AHA incorporation and fewer proteins identified in the mass spectrometry screen, as anticipated from prior work indicating an age-dependent decrease in translation in this AD mode[15]. At both timepoints, the vast majority (>85%) of measured proteins were synthesized consistently regardless of genotype, further illustrating the tight regulation of the proteome required for cell functioning. However, defined patterns of dysregulation were observed in APP/PS1 mice relative to unaffected littermates.

In young mice without extensive Aβ protein deposition, we observed a specific pattern of dysregulated protein synthesis, resulting in predominately decreased translation of proteins involved in a series of pathways critical to cell functioning. Of note, proteins involved in both protein degradation (via GO term ‘proteasome’) and protein synthesis (via GO term ‘ribosome’) showed dysregulated synthesis in the APP/PS1 hippocampus relative to wild-type littermates. In fact, the dysfunctional production of components of the proteasome could have a negative effect on ribosomal function and general protein synthesis, as an interplay between impaired proteasomal function and

translation has previously been described[17]. Dysregulated synthesis of synaptic proteins were also highlighted at this time point, which could underlie the decreased synaptic density previously observed in 4 month-old APP/PS1 mice[44], as well as the altered excitability observed by 4 months[37], and impaired synaptic transmission observed in APP/PS1 mice at 5 months of age[45]. Thus, our findings may represent a critical window in which modulation of translation limits synaptic changes that result in memory deficits later in disease progression.

When *de novo* protein synthesis was examined in 12+ month-old APP/PS1 mice that display pronounced AD-like pathology and memory impairment, a large number of mitochondrial proteins previously linked to AD were dysregulated. Mitochondrial structure and function is known to be compromised in human patients[46,47], but whether these deficits contribute to the disease or whether they are a biproduct of disease progression continues to be debated[48]. Alongside mitochondria, lysosomal protein synthesis was dysregulated in the symptomatic APP/PS1 mice. Increasing evidence suggests that lysosomal biogenesis is initially upregulated in early stages of AD[32], before progressive dysfunction throughout the disease process results in the accumulation of enlarged lysosomes, which fail to effectively degrade their contents[49].

A final significant pathway that was observed in the analysis of dysregulated proteins following symptom onset was constituents of the cytosolic ribosome, including eight ribosomal proteins and nucleolar protein of 40 kDa (Zcchc17). This zinc ion binding protein has recently been identified as a modulator of synaptic gene expression in AD[50]. Moreover, Zcchc17 is thought to be involved in ribosome biogenesis and maturation[51]. Two protein components of the ribosome that were differentially regulated in the mature

APP/PS1 tissue, Rpl13 (decreased BONLAC labelling compared to wild-type) and Rpl18 (upregulated in APP/PS1 mice) were selected for validation analyses in hippocampal lysates. The total expression of both proteins reflected the level of synthesis as detected in the mass spectrometry screen, indicating that these are biologically relevant changes that require further investigation. Rpl13 has recently been described as a 'core' ribosomal protein included in all actively translating ribosomes[52], and yet has also been shown to be dysregulated at the gene expression level in hippocampal tissue from severe AD patients[53]. Although no study has yet linked alterations in Rpl18 expression with AD pathology, recent analysis has indicated dysregulation of *Rpl18* gene expression occurs early in the AD process [54].

In order to determine the full impact of APP/PS1 mutations on protein synthesis in these mice, we examined the biological pathways that exhibited changes across pathology development as detected by hierarchical cluster analysis of all proteins detected in both age groups. This list was not limited to proteins identified by C-score analysis as significantly dysregulated, and included proteins detected in the majority of samples which showed a fold change of <20%. Several functional clusters emerged, indicating pathways specific to stage of pathology development. Two clusters were specifically upregulated in the symptomatic APP/PS1 mice, those associated with the GO terms 'protein processing in the endoplasmic reticulum (ER)' and 'mitochondrial part: electron transfer activity'. Increased synthesis of proteins, including Stub1/CHIP, Cat and Hsph1, which have previously been implicated in the AD process[55-57], indicate that the unfolded protein response (UPR), the physiological response to the ER stress, might be chronically activated later in disease. This finding is consistent with our previous studies

showing that reducing the expression of PERK, an eIF2α kinase that triggers downregulation of protein synthesis in response to UPR activation, could restore hippocampal plasticity and memory deficits in symptomatic APP/PS1 mice[15].

Mitochondrial dysfunction is known to be an early event in both APP/PS1 mice[58] and human AD brain pathology[59-61], and is believed to play a role in the synaptic loss that occurs early in the disease process[62]. Downregulated synthesis of mitochondrial proteins, specifically the oxidative phosphorylation-associated proteins Ndufs5, Ndufa12, Cox4i1 and Cox6b in the younger APP/PS1 mice could underlie the decreased electron transport chain capacity observed in this and other models of AD-like pathology[63,64].

Functional clusters that exhibited downregulation in the aged APP/PS1 mice compared to the young cohort were also observed. The first cluster was associated with the GO term 'synapse', which may be a function of the decreased spine density previously observed in symptomatic APP/PS1 mice[44]. Proteins found in this hub included those involved in glutamatergic signaling, known to be impaired in both the human AD brain and APP/PS1 mice[65]. In addition, a cluster corresponding to 'glycolysis and gluconeogenesis' was decreased in the aged APP/PS1 hippocampal *de novo* proteome. Decreased glucose metabolism has been observed in the human AD brain using radioactive glucose labelling and PET scanning, and correlates well with AD-associated pathologies[66-68].

Although the cluster analysis described above examined general trends, we also conducted focused analysis using C-score-mediated detection of dramatic changes in *de novo* protein synthesis, where candidate proteins were selected for further analysis if they showed a fold-change of >20% in either direction in APP/PS1 mice vs. wild-type

littermates. Comparison of proteins selected in this manner revealed that although few proteins were dysregulated in both age groups, one third of these proteins were identified as ribosomal subunits. The ribosome is composed of four ribosomal RNA molecules and 80 ribosomal proteins[69], which together form the small and large ribosomal subunits that function together to translate mRNAs into proteins. Recent examination of *de novo* hippocampal protein synthesis following prolonged in vivo metabolic labelling revealed dysregulated synthesis of Rps3a[22]. Moreover, dysregulated expression of genes encoding several of the ribosomal proteins observed in our study (Rpl7, Rps6, Rps17 and Rps26) has previously been described in the AD brain[3]. Notably, decreased synthesis of ribosomal proteins is a common feature in both amyloid and tauopathy mouse models, as a recent *de novo* proteomic study using K3 and rTg4510 models of tauopathy revealed dysfunctional translation of these proteins[21].

The protein content of functional ribosomes was long thought to be largely homogenous, but recent studies have indicated sub-stoichiometric inclusion of ribosomal proteins in actively-translating ribosomes in mammalian cells[52,70]. In neurons, active remodeling of ribosomal protein content has been observed in response to axonal stimulation[71]. Notably, ribosomal protein gene expression is regulated throughout the aging process in the brain[72], indicating that the dynamic regulation of ribosomal components may play a role in cellular adaption to aging. Further, deficiency in particular ribosomal proteins results in hypersensitivity to deficits in the protein degradation system[73]. Importantly, the protein constituents of the actively translating ribosome appear to confer a level of preference for which mRNAs are translated, suggesting a further level of translational control[52]. Together with the aforementioned studies, our findings make a

strong case for further detailed investigations into the dysregulation of ribosomal protein synthesis and its subsequent consequences in AD.

One important consideration when using BONLAC labeling is that the primary output is the ratio of medium to heavy isotope labelling, which is used to generate the fold-changes that permit relative quantitation. A caveat to using this system in AD (in which translation is known to be impacted) is that if a protein is not synthesized at all during the labeling window, or synthesis levels are below detection in one sample within the pair, a ratio will not be generated. As we have observed, both here (Figure 1a) and previously[15,22], a significant decline in gross *de novo* protein synthesis in the APP/PS1 mouse[15,22], this inherent bias may have led to an exaggerated detection of upregulated vs. downregulated proteins in the symptomatic APP/PS1 hippocampal samples. Bioinformatic comparison of the *de novo* hippocampal proteome generated in this, and recent *in vivo* analysis[22], with the basal proteome could reveal proteins that were not synthesized over the labelling period and were thus precluded from BONLAC ratio generation. Further by combining BONLAC labelling and TMT sample multiplexing, the number of missing peptide quantification values in each sample is greatly reduced, providing deeper coverage of the *de novo* proteome[74]. The incorporation of this novel approach into subsequent studies promises to reveal new insights into the cellular processes that accompany pathology progression in the APP/PS1 mouse.

In summary, here we have illustrated a compelling picture of dysregulation of the *de novo* proteome in the APP/PS1 mouse model of AD-like amyloidy, throughout pathology development. Following validation of several candidate proteins to support the relevance of the changes observed in the mass spectrometry screen, we conducted

robust bioinformatic analysis of the newly made proteins. We observed dysregulated synthesis of proteins involved in several pathways known to be altered throughout the course of AD, including those involved in synaptic, mitochondrial and lysosomal functions, but we also observed significant disturbance of protein components of the ribosome. In light of recent research that indicates inclusion or exclusion of specific ribosomal subunits bestows selectivity to mRNA translation, the significant up- and down-regulation of ribosomal protein synthesis identified here, even prior to the development of pathology, may underly the progressive deterioration of cellular function and memory observed in this AD model, and in individuals with AD.

Materials and Methods

Animals

All procedure involving animals were performed in accordance with protocols approved by the New York University Animal Welfare Committee and followed the National Institutes of Health (NIH) *Guide for the Care and Use of Laboratory Animals.* All mice were housed in the New York University animal facility. Mice of both sexes were used. APP/PS1 transgenic mice (B6;C3-Tg(APPswe, PSEN1/dE9)85Dbo/Mmjax) and their wild-type littermates were bred and maintained on C57-BL6 and B6.C3 (Jackson Labs) backgrounds. Mice were housed with their littermates in groups of two to three animals per cage and kept on a 12-hour regular light/dark cycle, with food and water provided ad libitum. All genotypes were verified by polymerase chain reaction. Mice were used at an age of either 3-5 months or 12-15 months.

Immunohistochemistry

Mice were deeply anesthetized with ketamine (150 mg/kg) and transcardially perfused with 0.1M PBS followed by 4% PFA before brains were removed and post-fixed for 48 hours. 40 µm free-floating coronal sections containing the hippocampus were cut using a Leica vibratome, collected and stored at 4°C in 0.01% sodium azide until use. Sections were permeabilized in 0.5% Triton X-100 (15 min) prior to blocking (5% normal goat serum, 0.1% Triton X-100; 1 h). Slices were incubated overnight at 4°C in rabbit anti-amyloid beta antibody (1:200; clone 6E10, ENZ-ABS612-0200, Enzo Life Sciences), followed by Alexa-488-labelled goat anti-rabbit secondary antibody (1:500; RT, 1.5 h). Slices were mounted using ProLong Gold Antifade Mountant with DAPI. Tile-scan z stack images (10-15 optical sections depending on slice thickness) were collected using an SP8 confocal microscope (Leica) with a 20X magnification lens and Leica LASX software, with laser intensity, smart gain and offset maintained throughout the experiment. Images were processed using ImageJ 2.0.0 using the Bio-Formats importer plug-in. Plaque number was manually quantified using the Cell Counter plugin (*n* = 1-2 animals/group, 1 dorsal hippocampal slice/animal).

AHA and SILAC Dose

AHA and SILAC labels were used as previously described[23]. AHA was purchased from Click Chemistry Tools, AZ, USA, and SILAC amino acids (13C6-15N2-lysine, 13C6-15N4-arginine (Lys8/Arg10) and D4-lysine/13C6-arginine (Lys4/Arg6)) were obtained from Cambridge Isotope Laboratories, MA, USA and used at previously described concentrations[23,24]. Assignment of SILAC labels to experimental conditions (wild-type or

APP/PS1) was alternated between biological replicates to ensure that results were not biased by labelling.

Acute Hippocampal Slice Preparation and Incubation

400 µm transverse hippocampal slices were obtained as previously described[75-77]. Slices were recovered and incubated in ACSF for 20 min at room temperature, then at 32°C for 45 min. AHA (1 mM) and SILAC amino acids were added to the ACSF, and slices were incubated for 5 hrs. Following the labelling period, slices were immediately flash frozen for mass spectrometry and stored at - 80 °C until use.

BONLAC Sample Preparation for Mass Spectrometry.

Samples were prepared as previously described[23] using the Click-IT Protein Enrichment Kit (ThermoFisher Scientific). BONLAC was carried out with a minimum of five runs per condition, with each run examining hippocampal slices from one WT and one age-matched APP/PS1 animal (*n* = 5-7 biological replicates made up of 1 APP/PS1 and 1 WT; 5-7 animals of each age per genotype were used in total). Briefly, following labeling, equal weights of tissue from age-matched pairs of WT and APP/PS1 animals were lysed together in buffer containing 8 M urea, 200 mM Tris pH 8, 4% CHAPS, 1 M NaCl and protease inhibitor cocktail (cOmplete, Mini, Roche; two tablets per 10 mL of lysis buffer). The lysate was sonicated before AHA-labeled proteins were covalently coupled to alkyne-tagged agarose beads using reagents provided in the kit. Beads were washed repeatedly with SDS (1% SDS, 100 mM Tris pH 8, 250 mM NaCl and 5 mM EDTA) and alkyne-bound proteins were reduced with DTT at 70 °C before alkylation with iodoacetamide protected

from light at room temperature. Beads were then washed sequentially to remove non-specifically bound proteins with 100 column volume SDS wash buffer, 8 M urea, and finally with 20% acetonitrile. Bound proteins were digested on-resin with trypsin (Trypsin Gold, Mass spectrometry grade, Promega) at 37 °C overnight in 25 mM ammonium bicarbonate, and the resulting tryptic peptides were desalted using hand-packed StageTips[78]. Desalted peptides were dried to a small droplet, under vacuum, in a SpeedVac.

Liquid Chromatography and Mass Spectrometry

LC-MS was conducted using a Thermo Scientific EASY-nLC 1000 coupled to a Q Exactive, High Field mass spectrometer (ThermoFisher Scientific) equipped with a nanoelectrospray ionization source. Peptide separation was achieved with a self-packed ReproSil-Pur C18 AQ 3µ reverse phase column (Dr.Maisch GmbH, Germany, 75 µm inner ID, ~25cm long). Peptides were eluted via a gradient of 3 - 40% acetonitrile in 0.1% formic acid over 120 min at a flow rate of 250 nL/min at 45 °C, maintained with a column heater (Sonation GmbH, Germany). The mass spectrometer was operated in data-dependent mode with survey scans acquired at a resolution of 120,000 at m/z 400. Up to the top 15 most abundant precursors from the survey scan were selected with an isolation window of 1.6 Thomsons and fragmented by higher energy collisional dissociation with normalized collision energies of 27. The maximum ion injection times for the survey scan and the MS/MS scans were 60 ms, and the ion target value for both scan modes were set to 1,000,000.

Protein Identification and Quantitation

Raw files obtained from mass spectrometry runs were processed using the MaxQuant computational proteomics platform (Version 1.5.5.1[79]) for peptide identification and quantitation. Fragmentation spectra were searched against the Uniprot mouse protein database (downloaded on 12/20/2017, containing 16,950 non-redundant protein entries, combined with 262 common contaminants), allowing for up to two missed tryptic cleavages. Cysteine carbamidomethylation was set as a fixed modification, and methionine oxidation, acetylation of protein N-terminal, D-4 lysine, 13C6-arginine 13C6-15N2-lysine and 13C6-15N4-arginine were used as variable modifications for the database search. The mass tolerances were set to 7 ppm for precursor, and 10 ppm for fragment respectively. A false discovery rate (FDR) of 1% was applied to both peptide and protein identifications.

Data Availability

The raw mass spectrometry data generated during this study are available at MassIVE (Center for Computational Mass Spectrometry, University of California, San Diego) with the accession number (ftp://massive.ucsd.edu/MSV000085962/). Note to reviewers: data can be accessed prior to publication using the following details: User: MSV000085962; Password: a

Computational Processing of BONLAC MS data

MaxQuant-normalized H/M ratios (heavy vs. medium isotopes) were used for quantitative analysis. Ratios were inverted for experiments where isotopic labelling was reversed. A

custom-made *R* script was used to select protein candidates where the average ratio was above or below an arbitrary threshold of 20% (>0.8 or <1.2). Only proteins that were measured in the majority of samples and were consistently up- or down-regulated following manual examination of the dataset were selected. This method allows for non-biased selection of up- or down-regulated proteins, taking variation between replicates into account.

Protein Identity and Interaction Interpretation

Gene Ontology analysis was performed using the Database for Annotation, Visualization and Integrated Discovery (DAVID version 6.8)[80]. Candidate proteins selected according to the methods outlined above were added to the software as a 'gene list', and the background was considered as all proteins previously measured in hippocampal brain slices[23]. To depict the function clustering of the data described by DAVID, the STRING database (version 11.0) was used. This online resource contains both known and predicted protein-protein interactions[81]. Clusters of proteins of interest were highlighted for visualization, and FDR of GO term was noted.

For hierarchical clustering of datasets, Cytoscape (Version 3.71) was used. Datasets were uploaded to the program as lists of proteins, and STRING enrichment was conducted against the mouse genome. Fold change (average or individual APP/PS1:WT samples, as appropriate) were uploaded against the relevant network. Hierarchical clusters were generated using the clusterMaker plugin, with pairwise average linkage and Euclidean distance metric.

Western Blot Validation

All western blotting was carried out as previously described[82]. Briefly, hippocampal tissue reserved from samples prior to mass spectrometry processing was homogenized in lysis buffer protease and phosphatase inhibitors. Protein concentration was measured using BCA assay (Pierce). Aliquots of protein (20-40 µg) were separated using Bolt Bis-Tris gels (4-12%; Thermo Scientific) and transferred to a nitrocellulose membrane which was probed using appropriate primary and secondary antibody pairs. Membranes were washed and probed for total protein using MemCode Reversible Protein Stain (Thermo Scientific), before antibody signal was detected using chemiluminescence (GE Healthcare). Band density values were normalized to total protein as detected using MemCode. Mean band densities for samples from APP/PS1 mouse samples were normalized to corresponding samples from WT animals.

Statistics and Reproducibility

BONLAC analysis

Acute hippocampal slices from APP/PS1 and WT littermates were individually labelled with AHA and heavy or medium SILAC amino acids. Equal numbers of slices from each pair of APP/PS1 and WT mice (<5 slices/animal) were combined prior to BONCAT enrichment and mass spectrometry analysis. Between five to seven mass spectrometry runs per age group were conducted in this fashion (n = 5-7 paired biological replicates). Ratios of medium to heavy SILAC labelling were examined using MaxQuant, and protein candidates with an average fold change of ± 20% were identified in an unbiased manner using *R.* Proteins identified in this manner were then manually confirmed if they were

548 detected in the majority of samples, and showed the same trend (up- or downregulation)
549 in the majority of samples.
550
551 Western blot
552 AHA-labelled acute hippocampal slices were reserved from APP/PS1 and WT mice prior
553 to mass spectrometry analysis. Slices are from between 5-7 animals/genotype/age. Data
554 are expressed normalized to total protein, relative to WT levels, and shown as mean ±
555 SEM, with all data points shown to illustrate variability in distribution. Statistical
556 significance ($p < 0.05$) was calculated using Prism (Version 8.4.2). Differences between
557 groups were evaluated by two-tailed t-tests.
558
559 Simple linear regression modelling
560 To determine whether a linearity existed between the expression of *de novo* synthesized
561 and total candidate protein expression, we performed a linear regression analysis on the
562 data described above using Prism. We fit a curve using the simple linear regression
563 model, and determined whether the relationship was significantly non-zero ($p < 0.05$). For
564 visual comparison, we also traced an absolute correlation ($r^2 = 1$).
565
566 *Antibodies*
567 The following antibodies were used in this study: rabbit anti-APP monoclonal antibody
568 (1:1000; clone Y188, ab32136, Abcam), mouse anti-cathepsin-d monoclonal antibody
569 (1:500; clone CTD-19, ab6313, Abcam), rabbit anti-GAP-43 polyclonal antibody (1:500;
570 ab5220, Sigma), anti-Rpl13 polyclonal antibody (1:1000; PA5-41715, Thermofisher), and

anti-Rpl18 polyclonal antibody (1:5000; ab241988, Abcam). Secondary antibodies were either goat anti-mouse IgG HRP or goat anti-rabbit IgG HRP (Promega; 1:10,000) respectively.

Acknowledgments

The authors acknowledge Dr. Francesco Longo for his assistance with hippocampal slice preparation and Dr. Heather Bowling for her contributions to the experimental design.

Author Contributions

M.K.E., H.E-B., T.A.N. and E.K. designed the study. M.K.E., H.E-B., M.M.O. and M.M. performed research. M.K.E. and H.E-B analyzed data. H.E-B., T.A.N and E.K. contributed reagents, materials, animals and analysis tools. M.K.E., H.E-B., M.M.O., T.A.N. and E.K analyzed and discussed results. M.K.E. and E.K. wrote the manuscript, with input from other authors.

Competing interests

The authors declare no competing interests.

References

1 Alzheimer, A. Uber eine eigenartige Erkrankung der Hirnrinde. *Zentralbl. Nervenh. Psych.* **18**, 177-179 (1907).

2 Scahill, R. I., Schott, J. M., Stevens, J. M., Rossor, M. N. & Fox, N. C. Mapping the evolution of regional atrophy in Alzheimer's disease: unbiased analysis of fluid-registered serial MRI. *Proc Natl Acad Sci U S A* **99**, 4703-4707, doi:10.1073/pnas.052587399 (2002).

3 Hernández-Ortega, K., Garcia-Esparcia, P., Gil, L., Lucas, J. J. & Ferrer, I. Altered machinery of protein synthesis in Alzheimer's: from the nucleolus to the ribosome. *brain pathology* **26**, 593-605 (2016).

4 Kaushik, S. & Cuervo, A. M. Proteostasis and aging. *Nature Medicine* **21**, 1406-1415, doi:10.1038/nm.4001 (2015).
5 Ciechanover, A. & Kwon, Y. T. Degradation of misfolded proteins in neurodegenerative diseases: therapeutic targets and strategies. *Experimental & Molecular Medicine* **47**, e147-e147, doi:10.1038/emm.2014.117 (2015).
6 Keller, J. N., Hanni, K. B. & Markesbery, W. R. Impaired proteasome function in Alzheimer's disease. *Journal of neurochemistry* **75**, 436-439 (2000).
7 Mawuenyega, K. G. *et al.* Decreased clearance of CNS β-amyloid in Alzheimer's disease. *Science* **330**, 1774-1774 (2010).
8 Holt, C. E., Martin, K. C. & Schuman, E. M. Local translation in neurons: visualization and function. *Nature Structural & Molecular Biology* **26**, 557-566, doi:10.1038/s41594-019-0263-5 (2019).
9 Richter, J. D. & Klann, E. Making synaptic plasticity and memory last: mechanisms of translational regulation. *Genes & development* **23**, 1-11 (2009).
10 Costa-Mattioli, M., Sossin, W. S., Klann, E. & Sonenberg, N. Translational control of long-lasting synaptic plasticity and memory. *Neuron* **61**, 10-26 (2009).
11 An, W.-L. *et al.* Up-regulation of phosphorylated/activated p70 S6 kinase and its relationship to neurofibrillary pathology in Alzheimer's disease. *The American journal of pathology* **163**, 591-607 (2003).
12 Chang, R. C., Wong, A. K., Ng, H.-K. & Hugon, J. Phosphorylation of eukaryotic initiation factor-2α (eIF2α) is associated with neuronal degeneration in Alzheimer's disease. *Neuroreport* **13**, 2429-2432 (2002).
13 Ferrer, I. Differential expression of phosphorylated translation initiation factor 2 alpha in Alzheimer's disease and Creutzfeldt–Jakob's disease. *Neuropathology and applied neurobiology* **28**, 441-451 (2002).
14 Li, X. *et al.* Phosphorylated eukaryotic translation factor 4E is elevated in Alzheimer brain. *Neuroreport* **15**, 2237-2240 (2004).
15 Ma, T. *et al.* Suppression of eIF2α kinases alleviates Alzheimer's disease–related plasticity and memory deficits. *Nature neuroscience* **16**, 1299 (2013).
16 Lourenco, M. V. *et al.* TNF-α mediates PKR-dependent memory impairment and brain IRS-1 inhibition induced by Alzheimer's β-amyloid oligomers in mice and monkeys. *Cell metabolism* **18**, 831-843 (2013).
17 Ding, Q., Markesbery, W. R., Chen, Q., Li, F. & Keller, J. N. Ribosome dysfunction is an early event in Alzheimer's disease. *Journal of Neuroscience* **25**, 9171-9175 (2005).
18 Langstrom, N., Anderson, J., Lindroos, H., Winbland, B. & Wallace, W. Alzheimer's disease-associated reduction of polysomal mRNA translation. *Molecular Brain Research* **5**, 259-269 (1989).
19 Sajdel-Sulkowska, E. M. & Marotta, C. A. Alzheimer's disease brain: alterations in RNA levels and in a ribonuclease-inhibitor complex. *Science* **225**, 947-949 (1984).
20 Buffington, S. A., Huang, W. & Costa-Mattioli, M. Translational control in synaptic plasticity and cognitive dysfunction. *Annual review of neuroscience* **37**, 17-38 (2014).
21 Evans, H. T., Benetatos, J., van Roijen, M., Bodea, L. G. & Götz, J. Decreased synthesis of ribosomal proteins in tauopathy revealed by non-canonical amino acid labelling. *The EMBO journal* **38**, e101174 (2019).

22 Ma, Y., McClatchy, D. B., Martínez-Bartolomé, S., Bamberger, C. & Yates, J. R. A Temporal Quantitative Profiling of Newly Synthesized Proteins during Aβ Accumulation. *bioRxiv*, 2020.2001.2014.906560, doi:10.1101/2020.01.14.906560 (2020).
23 Bowling, H. *et al.* BONLAC: A combinatorial proteomic technique to measure stimulus-induced translational profiles in brain slices. *Neuropharmacology* **100**, 76-89 (2016).
24 Zhang, G. *et al.* In-depth quantitative proteomic analysis of de novo protein synthesis induced by brain-derived neurotrophic factor. *Journal of proteome research* **13**, 5707-5714 (2014).
25 Eichelbaum, K., Winter, M., Berriel Diaz, M., Herzig, S. & Krijgsveld, J. Selective enrichment of newly synthesized proteins for quantitative secretome analysis. *Nat Biotechnol* **30**, 984-990, doi:10.1038/nbt.2356 (2012).
26 Dieterich, D. C., Link, A. J., Graumann, J., Tirrell, D. A. & Schuman, E. M. Selective identification of newly synthesized proteins in mammalian cells using bioorthogonal noncanonical amino acid tagging (BONCAT). *Proceedings of the National Academy of Sciences* **103**, 9482, doi:10.1073/pnas.0601637103 (2006).
27 Ong, S. E. *et al.* Stable isotope labeling by amino acids in cell culture, SILAC, as a simple and accurate approach to expression proteomics. *Mol Cell Proteomics* **1**, 376-386, doi:10.1074/mcp.m200025-mcp200 (2002).
28 Bowling, H. *et al.* Altered steady state and activity-dependent de novo protein expression in fragile X syndrome. *Nature Communications* **10**, 1710, doi:10.1038/s41467-019-09553-8 (2019).
29 Volianskis, A., Køstner, R., Mølgaard, M., Hass, S. & Jensen, M. S. Episodic memory deficits are not related to altered glutamatergic synaptic transmission and plasticity in the CA1 hippocampus of the APPswe/PS1δE9-deleted transgenic mice model of ß-amyloidosis. *Neurobiol Aging* **31**, 1173-1187, doi:10.1016/j.neurobiolaging.2008.08.005 (2010).
30 Beckelman, B. C. *et al.* Genetic reduction of eEF2 kinase alleviates pathophysiology in Alzheimer's disease model mice. *J Clin Invest* **129**, 820-833, doi:10.1172/JCI122954 (2019).
31 Radde, R. *et al.* Abeta42-driven cerebral amyloidosis in transgenic mice reveals early and robust pathology. *EMBO Rep* **7**, 940-946, doi:10.1038/sj.embor.7400784 (2006).
32 Cataldo, A. M. *et al.* Gene expression and cellular content of cathepsin D in Alzheimer's disease brain: evidence for early up-regulation of the endosomal-lysosomal system. *Neuron* **14**, 671-680 (1995).
33 Hamazaki, H. Cathepsin D is involved in the clearance of Alzheimer's β-amyloid protein. *FEBS letters* **396**, 139-142 (1996).
34 Bogdanovic, N., Davidsson, P., Volkmann, I., Winblad, B. & Blennow, K. Growth-associated protein GAP-43 in the frontal cortex and in the hippocampus in Alzheimer's disease: an immunohistochemical and quantitative study. *Journal of neural transmission* **107**, 463-478 (2000).
35 de la Monte, S. M., Ng, S. C. & Hsu, D. W. Aberrant GAP-43 gene expression in Alzheimer's disease. *The American journal of pathology* **147**, 934-946 (1995).
36 Alonso-Nanclares, L., Merino-Serrais, P., Gonzalez, S. & DeFelipe, J. Synaptic changes in the dentate gyrus of APP/PS1 transgenic mice revealed by electron microscopy. *J Neuropathol Exp Neurol* **72**, 386-395, doi:10.1097/NEN.0b013e31828d41ec (2013).

37 Minkeviciene, R. *et al.* Amyloid beta-induced neuronal hyperexcitability triggers progressive epilepsy. *The Journal of neuroscience : the official journal of the Society for Neuroscience* **29**, 3453-3462, doi:10.1523/JNEUROSCI.5215-08.2009 (2009).

38 Gengler, S., Hamilton, A. & Hölscher, C. Synaptic plasticity in the hippocampus of a APP/PS1 mouse model of Alzheimer's disease is impaired in old but not young mice. *PLoS One* **5**, e9764-e9764, doi:10.1371/journal.pone.0009764 (2010).

39 Serneels, L. *et al.* gamma-Secretase heterogeneity in the Aph1 subunit: relevance for Alzheimer's disease. *Science (New York, N.Y.)* **324**, 639-642, doi:10.1126/science.1171176 (2009).

40 Park, J. H. *et al.* Subcutaneous Nogo Receptor Removes Brain Amyloid-β and Improves Spatial Memory in Alzheimer's Transgenic Mice. *The Journal of Neuroscience* **26**, 13279-13286, doi:10.1523/jneurosci.4504-06.2006 (2006).

41 Xu, Z.-Q. *et al.* Aerobic exercise combined with antioxidative treatment does not counteract moderate- or mid-stage Alzheimer-like pathophysiology of APP/PS1 mice. *CNS Neurosci Ther* **19**, 795-803, doi:10.1111/cns.12139 (2013).

42 Gruart, A., López-Ramos, J. C., Muñoz, M. D. & Delgado-García, J. M. Aged wild-type and APP, PS1, and APP + PS1 mice present similar deficits in associative learning and synaptic plasticity independent of amyloid load. *Neurobiol Dis* **30**, 439-450, doi:10.1016/j.nbd.2008.03.001 (2008).

43 Trinchese, F. *et al.* Progressive age-related development of Alzheimer-like pathology in APP/PS1 mice. *Annals of Neurology: Official Journal of the American Neurological Association and the Child Neurology Society* **55**, 801-814 (2004).

44 Smith, D. L., Pozueta, J., Gong, B., Arancio, O. & Shelanski, M. Reversal of long-term dendritic spine alterations in Alzheimer disease models. *Proceedings of the National Academy of Sciences* **106**, 16877, doi:10.1073/pnas.0908706106 (2009).

45 Zhang, H. *et al.* Synaptic fatigue is more pronounced in the APP/PS1 transgenic mouse model of Alzheimer's disease. *Current Alzheimer Research* **2**, 137-140 (2005).

46 Hirai, K. *et al.* Mitochondrial abnormalities in Alzheimer's disease. *The Journal of neuroscience : the official journal of the Society for Neuroscience* **21**, 3017-3023, doi:10.1523/JNEUROSCI.21-09-03017.2001 (2001).

47 Baloyannis, S. J. Mitochondrial alterations in Alzheimer's disease. *Journal of Alzheimer's disease* **9**, 119-126 (2006).

48 Swerdlow, R. H. Mitochondria and Mitochondrial Cascades in Alzheimer's Disease. *J Alzheimers Dis* **62**, 1403-1416, doi:10.3233/JAD-170585 (2018).

49 Nixon, R. A. Amyloid precursor protein and endosomal-lysosomal dysfunction in Alzheimer's disease: inseparable partners in a multifactorial disease. *The FASEB Journal* **31**, 2729-2743, doi:10.1096/fj.201700359 (2017).

50 Tomljanovic, Z., Patel, M., Shin, W., Califano, A. & Teich, A. F. ZCCHC17 is a master regulator of synaptic gene expression in Alzheimer's disease. *Bioinformatics* **34**, 367-371, doi:10.1093/bioinformatics/btx608 (2018).

51 Chang, W.-L. *et al.* Molecular characterization of a novel nucleolar protein, pNO40. *Biochemical and Biophysical Research Communications* **307**, 569-577, doi:https://doi.org/10.1016/S0006-291X(03)01208-7 (2003).

52 Shi, Z. *et al.* Heterogeneous ribosomes preferentially translate distinct subpools of mRNAs genome-wide. *Molecular cell* **67**, 71-83. e77 (2017).
53 Kong, W. *et al.* Independent component analysis of Alzheimer's DNA microarray gene expression data. *Molecular Neurodegeneration* **4**, 5, doi:10.1186/1750-1326-4-5 (2009).
54 Martínez-Ballesteros, M., García-Heredia, J. M., Nepomuceno-Chamorro, I. A. & Riquelme-Santos, J. C. Machine learning techniques to discover genes with potential prognosis role in Alzheimer's disease using different biological sources. *Information Fusion* **36**, 114-129 (2017).
55 Singh, A. K. & Pati, U. CHIP stabilizes amyloid precursor protein via proteasomal degradation and p53-mediated trans-repression of β-secretase. *Aging Cell* **14**, 595-604, doi:10.1111/acel.12335 (2015).
56 Habib, L. K., Lee, M. T. C. & Yang, J. Inhibitors of catalase-amyloid interactions protect cells from beta-amyloid-induced oxidative stress and toxicity. *J Biol Chem* **285**, 38933-38943, doi:10.1074/jbc.M110.132860 (2010).
57 Poirier, Y., Grimm, A., Schmitt, K. & Eckert, A. Link between the unfolded protein response and dysregulation of mitochondrial bioenergetics in Alzheimer's disease. *Cellular and Molecular Life Sciences* **76**, 1419-1431, doi:10.1007/s00018-019-03009-4 (2019).
58 Chen, L. *et al.* Studies on APP metabolism related to age-associated mitochondrial dysfunction in APP/PS1 transgenic mice. *Aging (Albany NY)* **11**, 10242-10251, doi:10.18632/aging.102451 (2019).
59 Hauptmann, S. *et al.* Mitochondrial dysfunction: an early event in Alzheimer pathology accumulates with age in AD transgenic mice. *Neurobiology of aging* **30**, 1574-1586 (2009).
60 Moreira, P. I., Santos, M. S. & Oliveira, C. R. Alzheimer's disease: a lesson from mitochondrial dysfunction. *Antioxidants & redox signaling* **9**, 1621-1630 (2007).
61 Nunomura, A. *et al.* Oxidative damage is the earliest event in Alzheimer disease. *Journal of Neuropathology & Experimental Neurology* **60**, 759-767 (2001).
62 Du, H., Guo, L. & Yan, S. S. Synaptic mitochondrial pathology in Alzheimer's disease. *Antioxidants & redox signaling* **16**, 1467-1475 (2012).
63 Bo, H. *et al.* Exercise-induced neuroprotection of hippocampus in APP/PS1 transgenic mice via upregulation of mitochondrial 8-oxoguanine DNA glycosylase. *Oxidative medicine and cellular longevity* **2014** (2014).
64 David, D. C. *et al.* Proteomic and functional analyses reveal a mitochondrial dysfunction in P301L tau transgenic mice. *Journal of Biological Chemistry* **280**, 23802-23814 (2005).
65 Minkeviciene, R. *et al.* Age-related decrease in stimulated glutamate release and vesicular glutamate transporters in APP/PS1 transgenic and wild-type mice. *J Neurochem* **105**, 584-594, doi:10.1111/j.1471-4159.2007.05147.x (2008).
66 Martins, R. N. *et al.* Alzheimer's disease: a journey from amyloid peptides and oxidative stress, to biomarker technologies and disease prevention strategies—gains from AIBL and DIAN cohort studies. *Journal of Alzheimer's Disease* **62**, 965-992 (2018).
67 Markesbery, W. R. Neuropathologic alterations in mild cognitive impairment: a review. *Journal of Alzheimer's Disease* **19**, 221-228 (2010).
68 Landau, S. M. & Frosch, M. P. (AAN Enterprises, 2014).
69 Yoshihama, M. *et al.* The human ribosomal protein genes: sequencing and comparative analysis of 73 genes. *Genome Res* **12**, 379-390, doi:10.1101/gr.214202 (2002).

70 Slavov, N., Semrau, S., Airoldi, E., Budnik, B. & van Oudenaarden, A. Differential Stoichiometry among Core Ribosomal Proteins. *Cell Reports* **13**, 865-873, doi:https://doi.org/10.1016/j.celrep.2015.09.056 (2015).
71 Shigeoka, T. *et al.* On-Site Ribosome Remodeling by Locally Synthesized Ribosomal Proteins in Axons. *Cell Reports* **29**, 3605-3619.e3610, doi:https://doi.org/10.1016/j.celrep.2019.11.025 (2019).
72 Ximerakis, M. *et al.* Single-cell transcriptomic profiling of the aging mouse brain. *Nature neuroscience* **22**, 1696-1708 (2019).
73 McIntosh, K. B., Bhattacharya, A., Willis, I. M. & Warner, J. R. Eukaryotic cells producing ribosomes deficient in Rpl1 are hypersensitive to defects in the ubiquitin-proteasome system. *PLoS One* **6**, e23579 (2011).
74 Zecha, J. *et al.* TMT labeling for the masses: a robust and cost-efficient, in-solution labeling approach. *Molecular & Cellular Proteomics* **18**, 1468-1478 (2019).
75 Chévere-Torres, I. *et al.* Metabotropic glutamate receptor-dependent long-term depression is impaired due to elevated ERK signaling in the ΔRG mouse model of tuberous sclerosis complex. *Neurobiology of disease* **45**, 1101-1110 (2012).
76 Kaphzan, H. *et al.* Genetic reduction of the α1 subunit of Na/K-ATPase corrects multiple hippocampal phenotypes in Angelman syndrome. *Cell reports* **4**, 405-412 (2013).
77 Santini, E. *et al.* Mitochondrial superoxide contributes to hippocampal synaptic dysfunction and memory deficits in Angelman syndrome model mice. *Journal of Neuroscience* **35**, 16213-16220 (2015).
78 Rappsilber, J., Mann, M. & Ishihama, Y. Protocol for micro-purification, enrichment, pre-fractionation and storage of peptides for proteomics using StageTips. *Nature protocols* **2**, 1896 (2007).
79 Cox, J. & Mann, M. MaxQuant enables high peptide identification rates, individualized ppb-range mass accuracies and proteome-wide protein quantification. *Nature biotechnology* **26**, 1367-1372 (2008).
80 Sherman, B. T. & Lempicki, R. A. Systematic and integrative analysis of large gene lists using DAVID bioinformatics resources. *Nature protocols* **4**, 44-57 (2009).
81 Szklarczyk, D. *et al.* STRING v11: protein-protein association networks with increased coverage, supporting functional discovery in genome-wide experimental datasets. *Nucleic Acids Res* **47**, D607-d613, doi:10.1093/nar/gky1131 (2019).
82 Sharma, A. *et al.* Dysregulation of mTOR signaling in fragile X syndrome. *Journal of Neuroscience* **30**, 694-702 (2010).

Figures

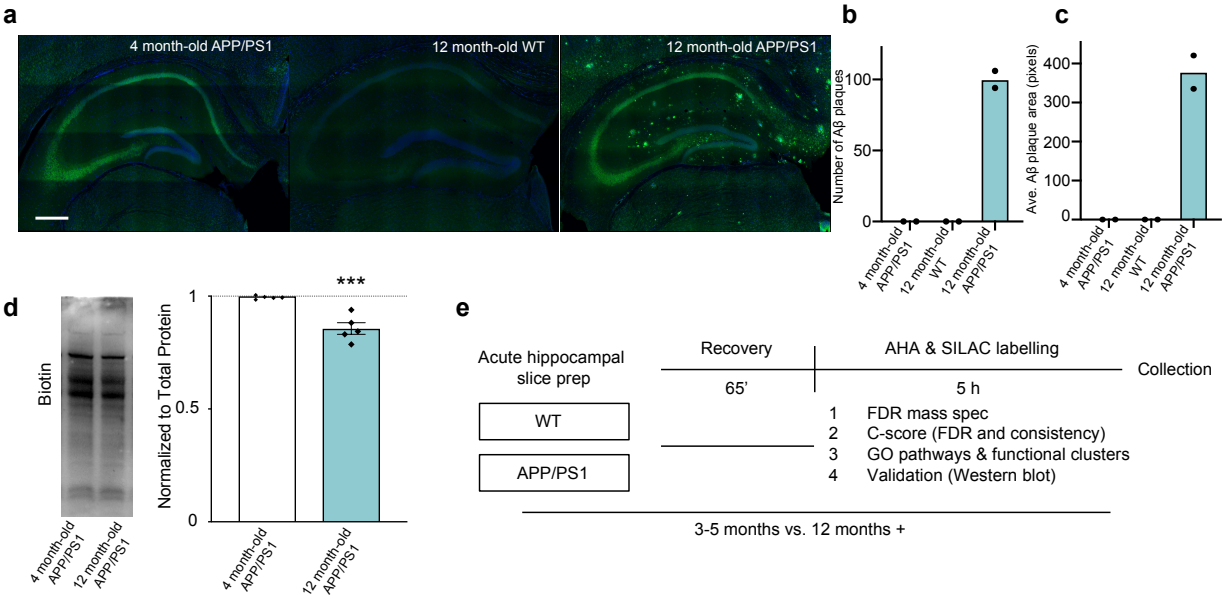

Figure 1. BONLAC-mediated labelling of *de novo* protein synthesis in the hippocampus of young and aged wild-type and APP/PS1 mice. a) Representative immunofluorescent images showing the progressive deposition of amyloid beta plaques in the hippocampus of 12 month-old APP/PS1 mice, but not 4 month-old APP/PS1 or 12 month-old wild-type (WT) mice (Blue = DAPI, Green = Aβ; scale bar = 50 μm). **b)** Quantification of the number of Aβ plaques in the hippocampus of 4 month-old APP/PS1 mice, 12 month-old WT and 12 month-old APP/PS1 mice. **c)** Quantification of the average area of the Aβ plaques observed in these groups (n = 1-2 mice per group for **b** and **c**). **d)** *De novo* synthesized protein in 3-5 month-old vs. 12+ month-old APP/PS1 mouse hippocampal slices as detected via AHA labelling, followed by biotin-alkyne click reaction and western blot (normalized to total protein (as determined via MemCode staining), expressed relative to average 4 month-old biotin signal; n = 5 mice/condition; error bars show mean ± SEM, statistical significance calculated using unpaired two tailed t test: t = 5.545, 95% confidence interval = -0.02033 to -0.08388, effect size = -0.1436 ± 0.0259, df = 8, p = 0.0005). **e)** Schematic showing BONLAC workflow for acute hippocampal slices from WT and APP/PS1 mice. Following labelling, slices from one APP/PS1 and one age-matched WT mouse are pooled for subsequent processing.

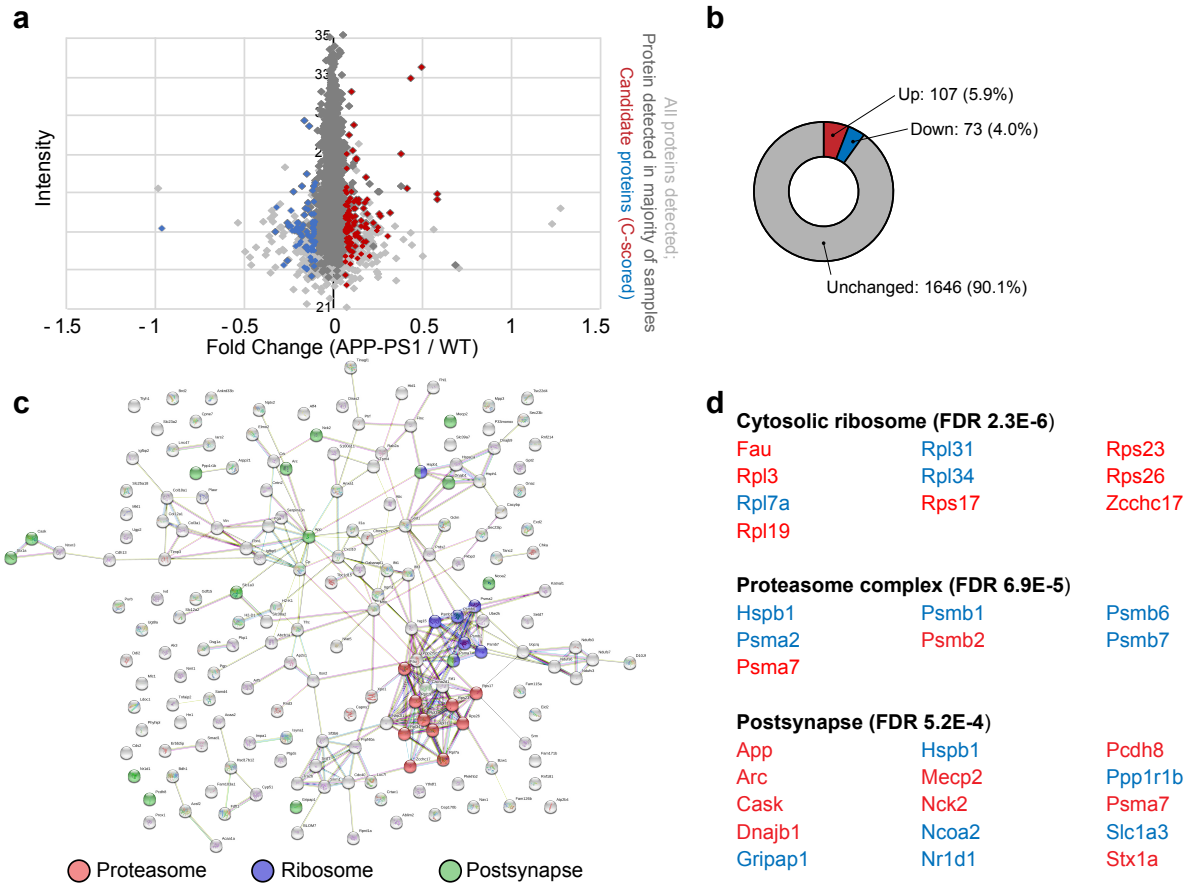

Figure 2. Steady state proteome differs in young wild-type and APP/PS1 mouse hippocampus. **a)** Fold change vs. intensity distribution plot of all newly made proteins detected in wild-type (WT) vs. 3-5 month-old APP/PS1 hippocampus (light grey), with proteins that were detected in majority of samples (>3 out of 5 samples; grey) and dysregulated candidate proteins identified by C-score screen (upregulated ≥ 20% in red, downregulated ≤ 20% in blue). **b)** Doughnut plot showing the proportion of detected proteins that were downregulated (fold change < 0.8, blue), upregulated (fold change > 1.2, red) or unchanged in the majority of 4 month-old APP/PS1 mice compared to WT littermates. **c)** String diagram depicting enriched gene ontology groups. **d)** Top functional clusters in 3-5 month-old APP/PS1 mice compared to WT using DAVID. Red = upregulated proteins. Blue = downregulated proteins.

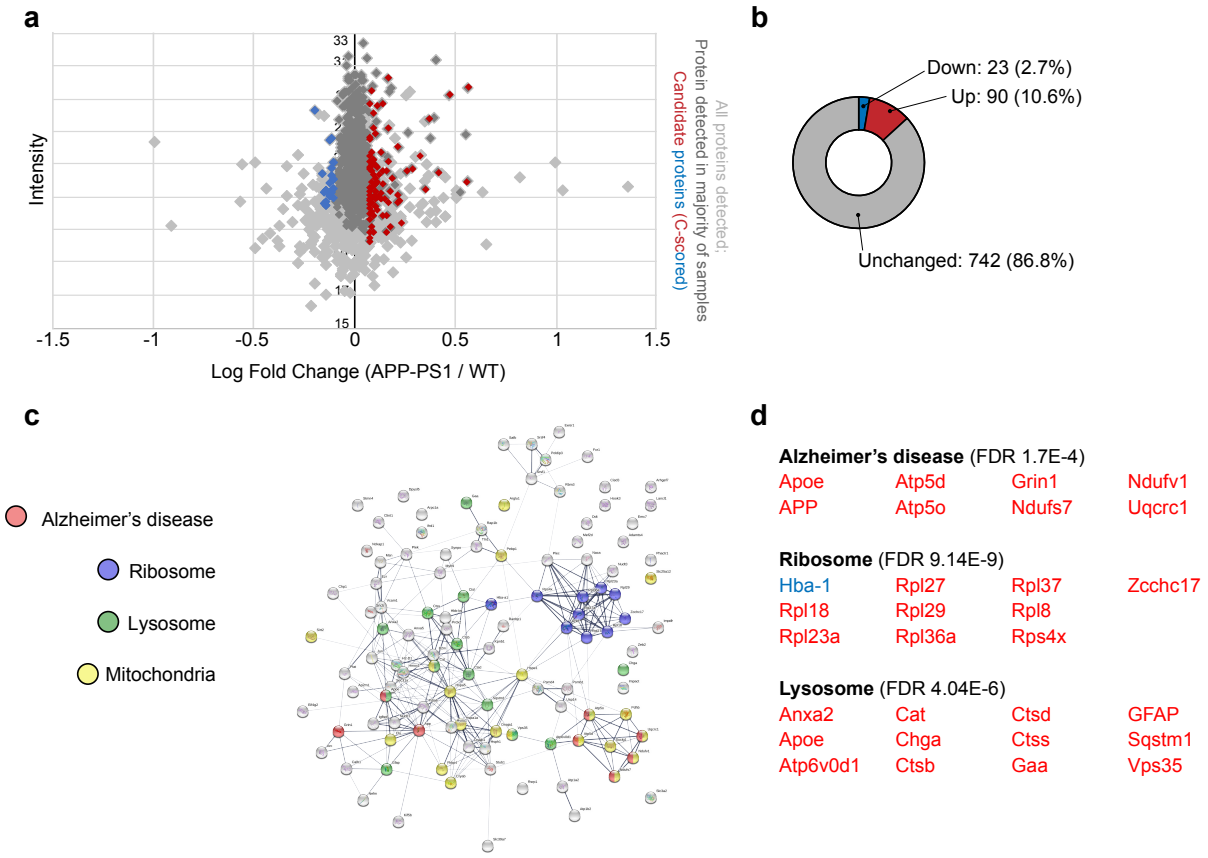

Figure 3. Analysis of altered *de novo* proteome highlights impaired proteostasis in aged APP/PS1 mice. a) Fold change vs. intensity distribution plot showing all proteins detected in 12+ month-old APP/PS1 mouse hippocampal slices vs. wild-type (WT) littermates using BONLAC (light grey). Dark grey overlay depicts proteins that were consistently detected in the majority of samples (>4/7), and candidate proteins identified by C-score screen as upregulated (fold change ≥ 1.2) shown in red, while downregulated proteins (≤ 0.8) are labelled blue. **b)** Doughnut plot indicating the majority of proteins detected in 12+ month-old mice are not altered in APP/PS1 mice (742; 86.8% of proteins detected). 23 proteins are downregulated compared to WT mice (2.7% of proteins show a fold change >0.8, blue) and 90 proteins are upregulated in APP/PS1 mice (10.6% of proteins show a fold change <1.2, red). **c)** String diagram showing enriched gene ontology networks. **d)** DAVID-identified functional clusters in 12+ month-old APP/PS1 mice. Red = upregulated proteins. Blue = downregulated proteins.

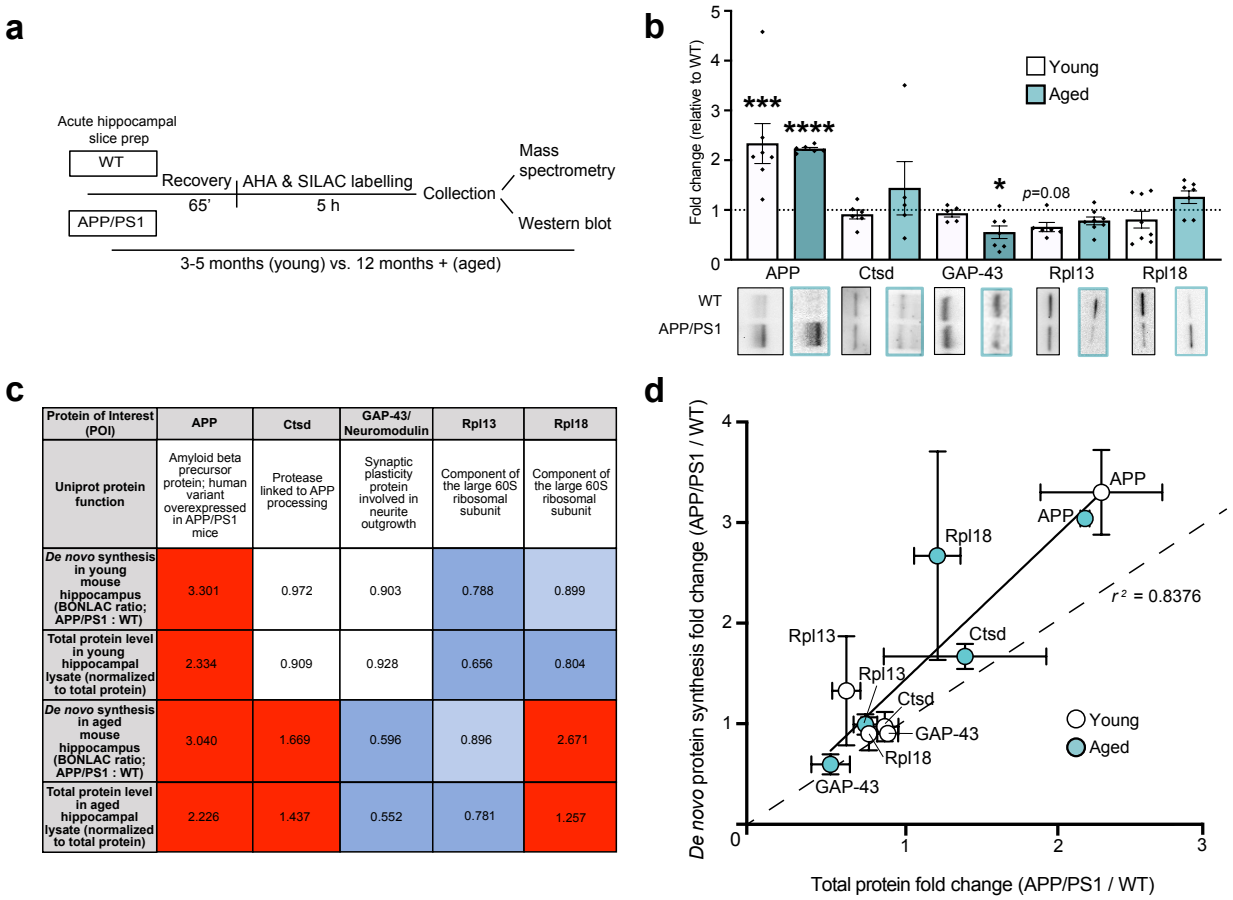

Protein of Interest (POI)	APP	Ctsd	GAP-43/ Neuromodulin	Rpl13	Rpl18
Uniprot protein function	Amyloid beta precursor protein; human variant overexpressed in APP/PS1 mice	Protease linked to APP processing	Synaptic plasticity protein involved in neurite outgrowth	Component of the large 60S ribosomal subunit	Component of the large 60S ribosomal subunit
De novo synthesis in young mouse hippocampus (BONLAC ratio; APP/PS1 : WT)	3.301	0.972	0.903	0.788	0.899
Total protein level in young hippocampal lysate (normalized to total protein)	2.334	0.909	0.928	0.656	0.804
De novo synthesis in aged mouse hippocampus (BONLAC ratio; APP/PS1 : WT)	3.040	1.669	0.596	0.896	2.671
Total protein level in aged hippocampal lysate (normalized to total protein)	2.226	1.437	0.552	0.781	1.257

Figure 4. Candidate proteins identified with BONLAC screen of *de novo* proteome exhibit altered expression levels in APP/PS1 mice. a) Schematic of workflow for slice allocation for mass spectrometry and western blot protein validation. **b)** Western blot quantitation of candidate proteins selected from BONLAC screen in 3-5 month-old (young; white bars) and 12+ month-old (aged; teal bars) mice, normalized to total protein (as assessed by MemCode) and expressed relative to wild-type (WT; n = 5-8 mice; error bars show mean ± SEM; statistical significance calculated between APP/PS1 and WT samples using unpaired two tailed t tests; young APP: t = 4.117, 95% confidence interval = 0.6495 to 2.028, effect size = 1.339 ± 0.3252, df = 16, p = 0.0008; aged APP: t = 15.29, 95% confidence interval =1.046 to 1.402, effect size = 1.224 ± 0.08007, df = 10, p < 0.0001; aged GAP-43: t = 2.266, 95% confidence interval = -0.9047 to -0.01774, effect size = -0.4612 ± 0.2035, df = 12, p = 0.0427; young Rpl13: t = 2.004, 95% confidence interval = -0.9413 to 0.07764, effect size = -0.4318 ± 0.2154, df = 7, p = 0.0851).; representative western blots showing selected protein levels in WT and APP/PS1 mouse hippocampal lysates (young: black box; aged: teal box). **c)** Comparison table showing average fold change in *de novo* synthesis of candidate proteins in young and aged APP/PS1 vs WT littermates as identified by BONLAC (young n=5; aged n=7) compared to change in total expression quantified by western blot. Vibrant color indicates value reached cutoff (+/- 20%; >0.8 or < 1.2); pale color indicates near threshold (within 5%); white indicates no change. **d)** Simple linear regression showing correlation between average *de novo* synthesized protein fold-change (as determined by BONLAC) vs. average total protein fold-change (as determined via western blot) of candidate proteins in the APP/PS1 vs. WT hippocampus at 3-5 months (white circles) and 12+ months of age (teal circles; figure shows mean ± SEM (vertical error bars: BONLAC; horizontal error bars: western blot); r^2 value = 0.8376, F = 41.25, DFn, DFd = 1, 8, p = 0.0002).

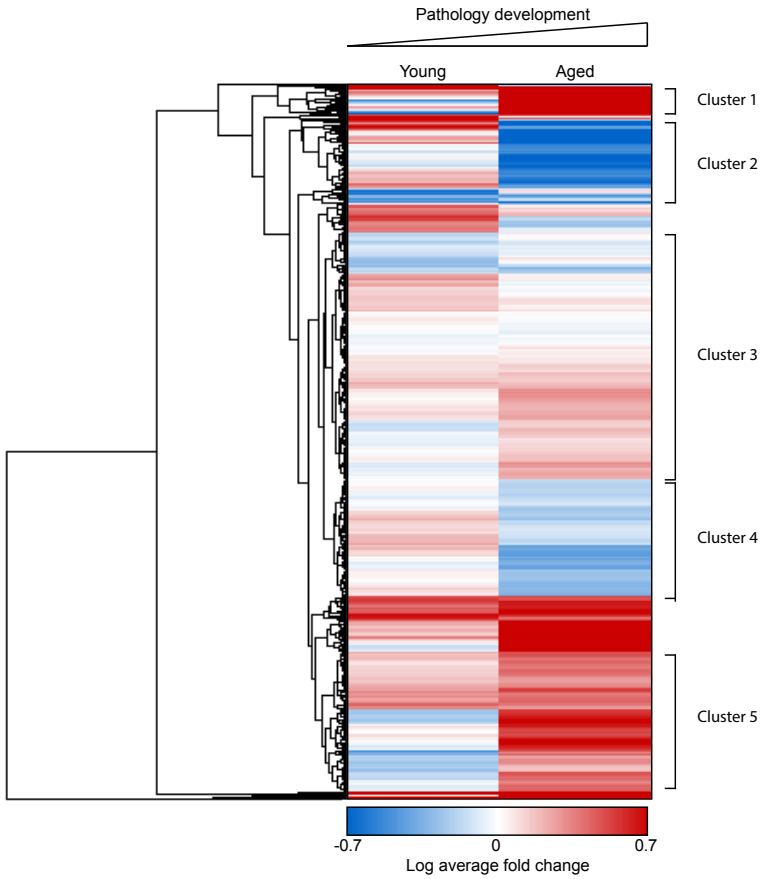

Figure 5. The biological pathways affected by dysregulated hippocampal protein synthesis vary with age in APP/PS1 mice. Hierarchical clustering heatmap reveals similarities and divergence in the mean-normalized log protein fold change of the 791 proteins detected in both young (3-5 months-old) and aged (12+ months-old) APP/PS1 mice relative to wild-type (WT) littermates. GO analysis evidenced 6 major clusters being significantly modified, which are: 1) protein processing in the endoplasmic reticulum (FDR 3.2E-04); 2) synapse (FDR 5.6E-07); 3) synaptic vesicle cycle (FDR 2.77E-06), membrane trafficking (FDR 6.24E-11) and synapse (FDR 4.82E-29); 4) axo-dendritic transport (FDR 4.86E-08) and glycolysis/gluconeogenesis (2.56E-05); 5) myelin sheath (5.17E-18) and Alzheimer's disease (8.16E-07); and 6) mitochondrial part (FDR 2.54E-08) and electron transfer activity (FDR 4.02E-05). FDR generated by StringDB algorithms. Red = upregulated proteins. Blue = downregulated proteins. White = unchanged protein expression.

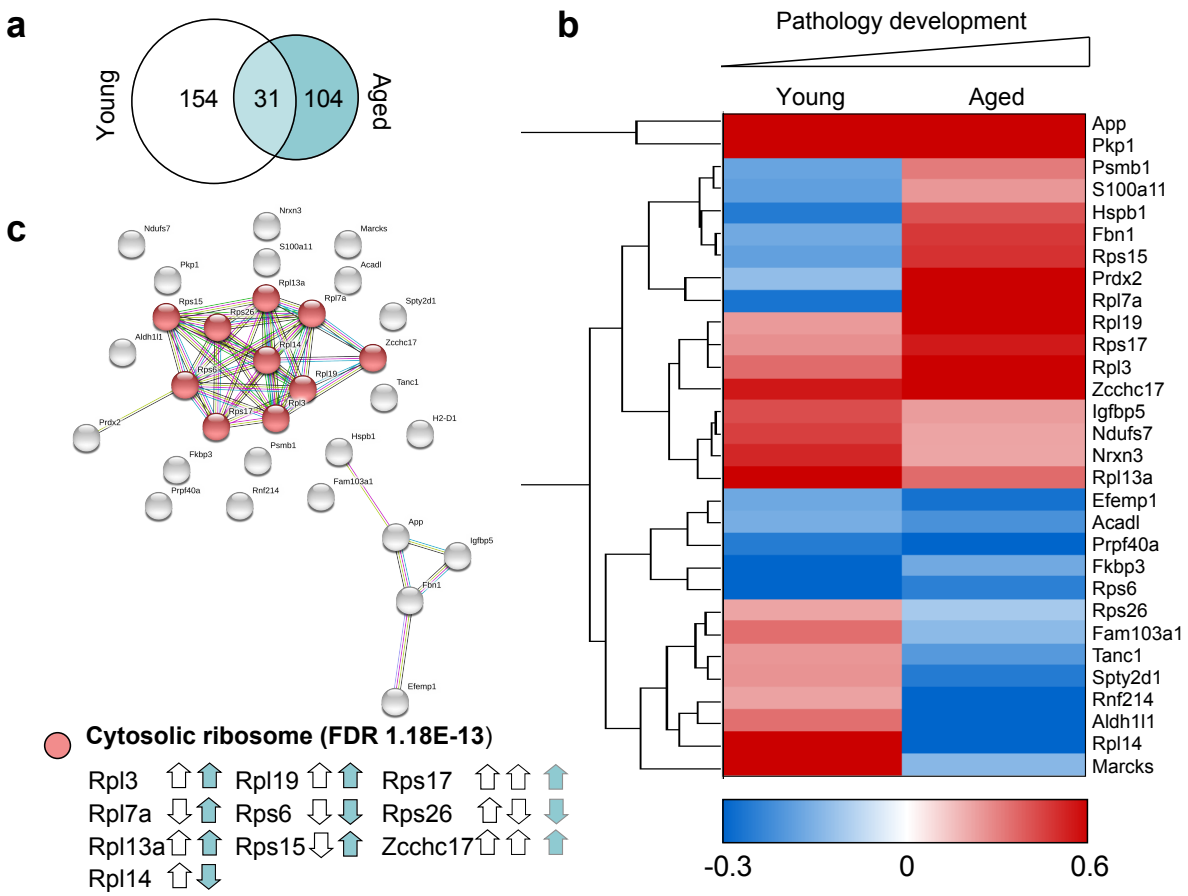

Figure 6. Steady state proteome is predominantly distinct throughout aging. a) Minimal overlap is observed between proteins that are dysregulated (as detected by C-score rank algorithm) in the hippocampi of 3-5 month-old (young) vs. 12+ month-old (aged) APP/PS1 mice. **b)** Hierarchical clustering of log fold changes reveals the majority of proteins which are dysregulated in both young and aged APP/PS1 mice compared to WT littermates do not show the same trend. Red = upregulated proteins. Blue = downregulated proteins. White = unchanged protein expression. **c)** String diagram revealing an enrichment of proteins in the GO network 'Cytosolic ribosome' in APP/PS1 throughout the aging process. White arrows = direction of regulation in young mice. Teal arrows = direction of regulation in aged mice.

Age-dependent shift in the *de novo* proteome accompanies pathogenesis in an Alzheimer's disease mouse model

Megan K. Elder[1], Hediye Erdjument-Bromage[2,3], Mauricio M. Oliveira[1], Maggie Mamcarz[1], Thomas A. Neubert[2,3], Eric Klann[1*]

Supplementary Figures 1-10
Supplementary Table 1

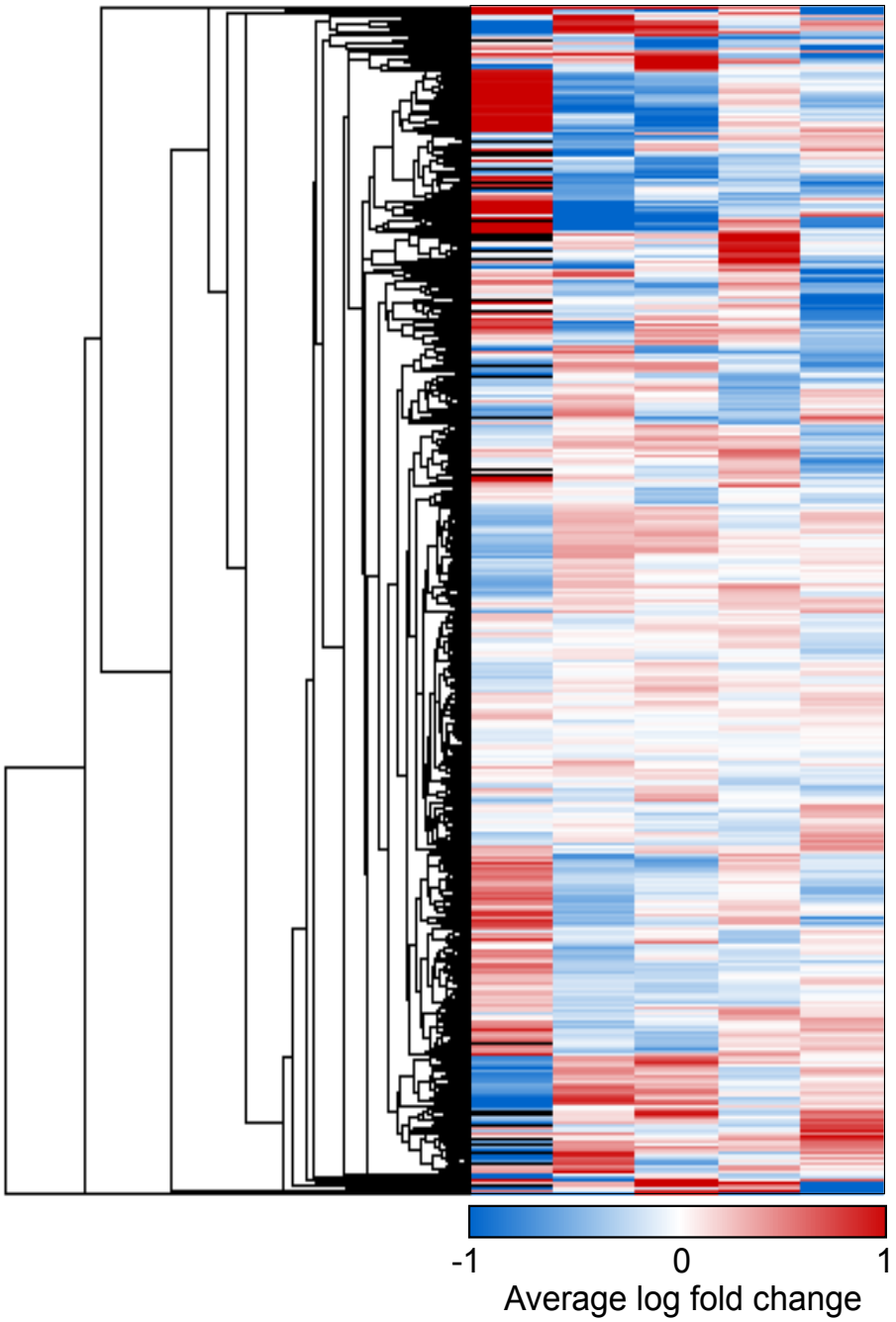

Supplementary Figure 1. All proteins detected in the young APP/PS1 hippocampus as detected by BONLAC. Hierarchical clustering-generated heatmap showing all protein fold-change ratios identified in at least one sample from the BONLAC screen. Red indicates proteins who show higher levels of *de novo* synthesis in ~4 month-old APP/PS1 mice compared to wild-type (WT) littermates, while downregulated proteins are shown in blue. White = no change. Black = MaxQuant ratio not calculated.

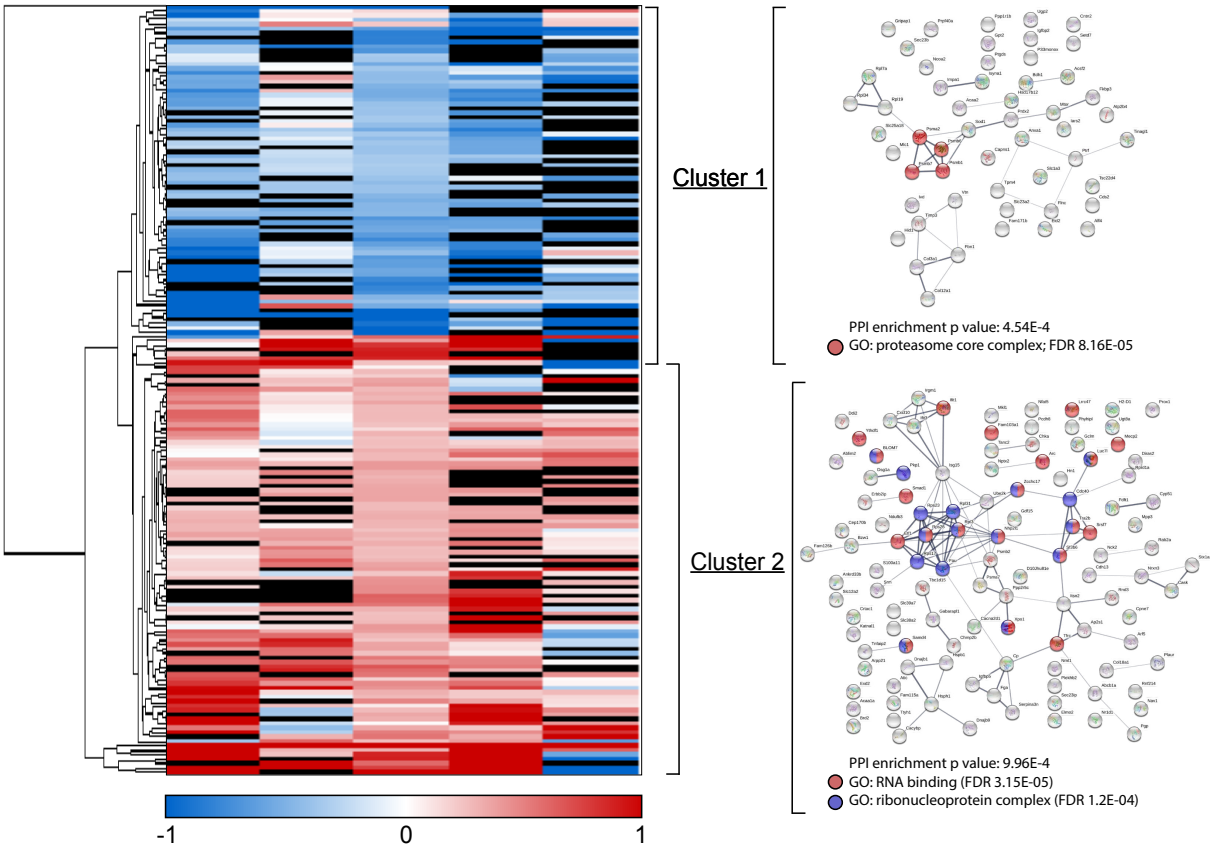

Supplementary Figure 2. Dysregulated protein candidates in the young APP/PS1 hippocampus as detected by BONLAC. Hierarchical clustered heatmap showing all candidate proteins identified from the BONLAC screen of ~4 months-old APP/PS1 vs. wild-type (WT) ranked by automated C-score. Protein candidates were identified by *R* script as showing an average fold change across all samples of ± 20% (<0.8 or >1.2). Manual validation confirmed candidates were detected in the majority of samples (>3/5), and that majority of samples showed the same trend (>50% either <0.79 or >1.19). Nodes in blue indicate downregulation, while red indicates increased *de novo* synthesis in the young APP/PS1 mice compared to WT littermates. Protein clusters are represented visually by String diagrams (right), with key pathways highlighted. White = no change. Black = MaxQuant ratio not calculated.

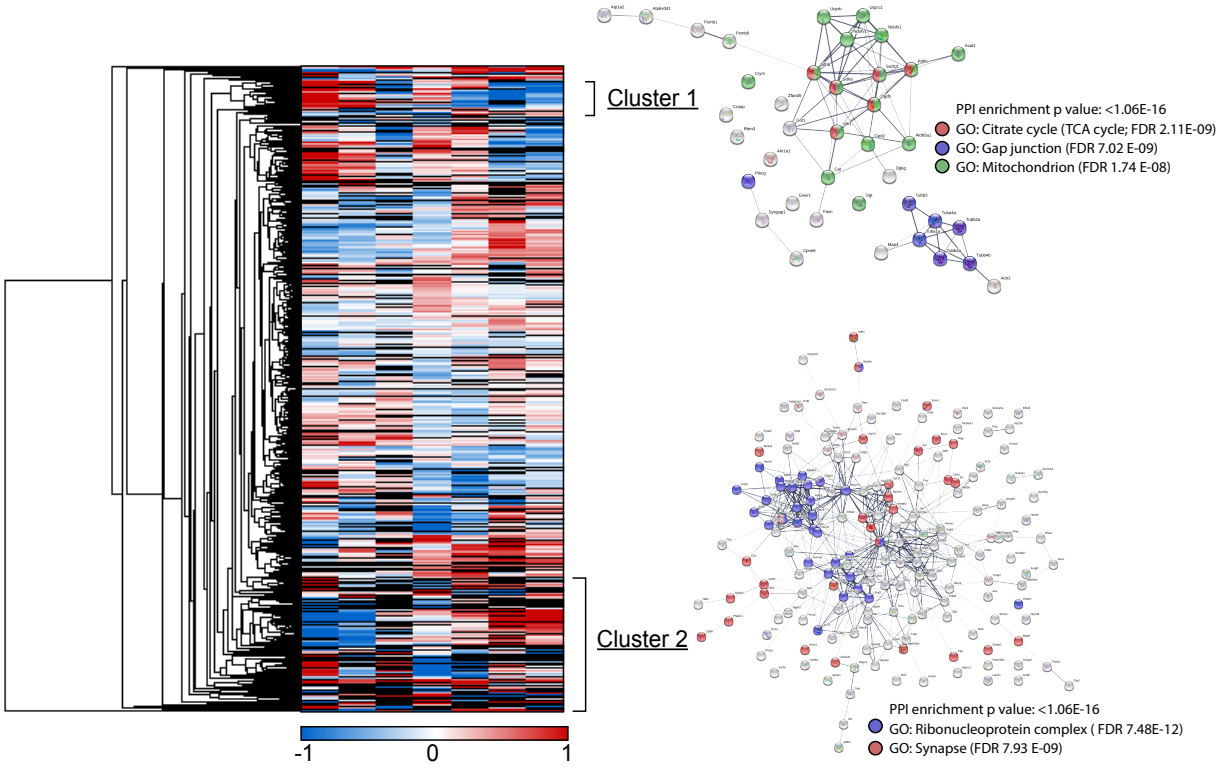

Supplementary Figure 3. All proteins detected in the aged APP/PS1 hippocampus as detected by BONLAC. Hierarchical clustering heatmap showing all protein fold-change ratios identified in the majority of samples from the BONLAC screen. Red indicates proteins which show higher levels of *de novo* synthesis in 12+ month-old APP/PS1 mice compared to WT littermates (APP is highlighted in top left), while downregulated proteins are shown in blue. String diagram of selected cluster is shown on right. White = no change. Black = MaxQuant ratio not calculated.

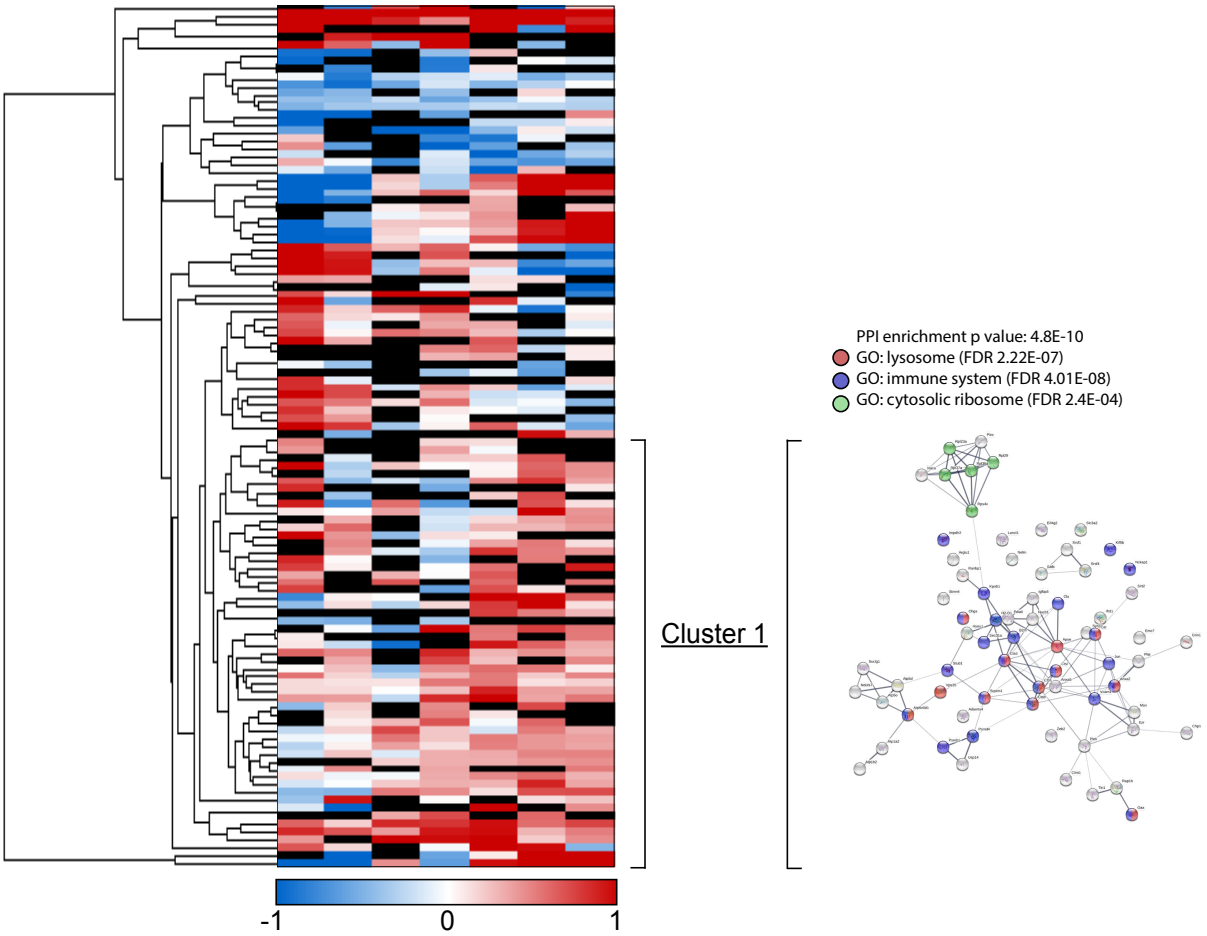

Supplementary Figure 4. Dysregulated protein candidates in the hippocampus of aged APP/PS1 mice as detected by BONLAC. Hierarchical clustered heatmap of candidate proteins identified from the BONLAC screen ranked by automated C-score. Protein candidates were identified by customized *R* script as showing an average fold change across all samples of ± 20% (<0.8 or >1.2). Manual validation confirmed candidates were detected in the majority of samples (>4/7), and that majority of samples showed the same trend (>50% either <0.79 or >1.19). String diagram representing main clusters shown on right, with key pathways highlighted. Black cells indicate absence of ratio. Red = upregulated proteins. Blue = downregulated proteins. White = no change. Black = MaxQuant ratio not calculated.

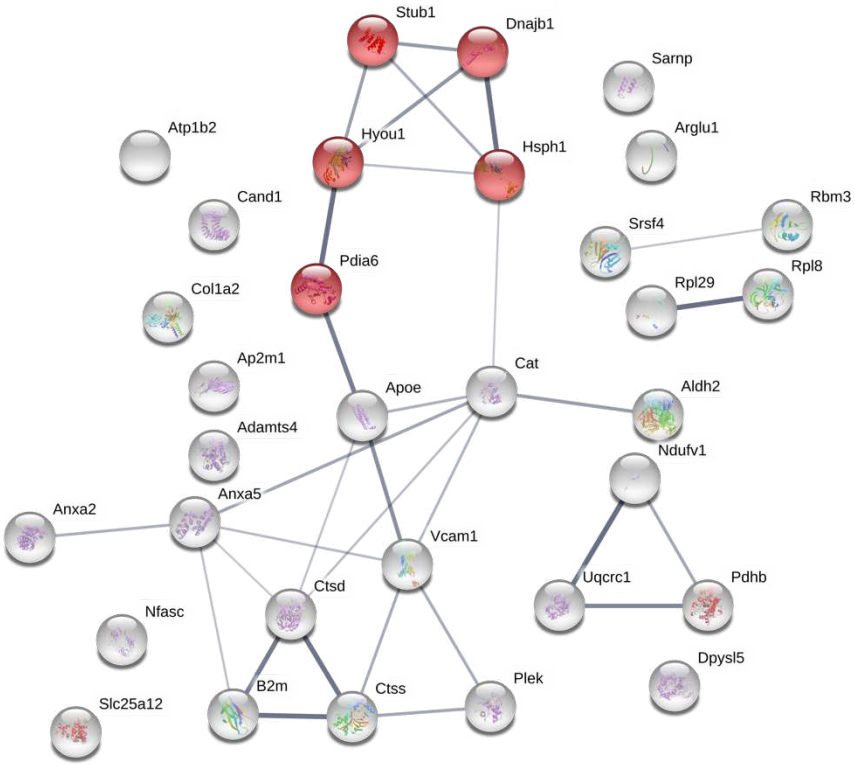

Supplementary Figure 5. Visual depiction of proteins in Hierarchical Cluster 1 (from Figure 5). String diagram showing biological networks between the proteins identified in Cluster 1. Figure generated by StringDb; Red node = GO: Protein processing in the endoplasmic reticulum; FDR:3.2E-4.

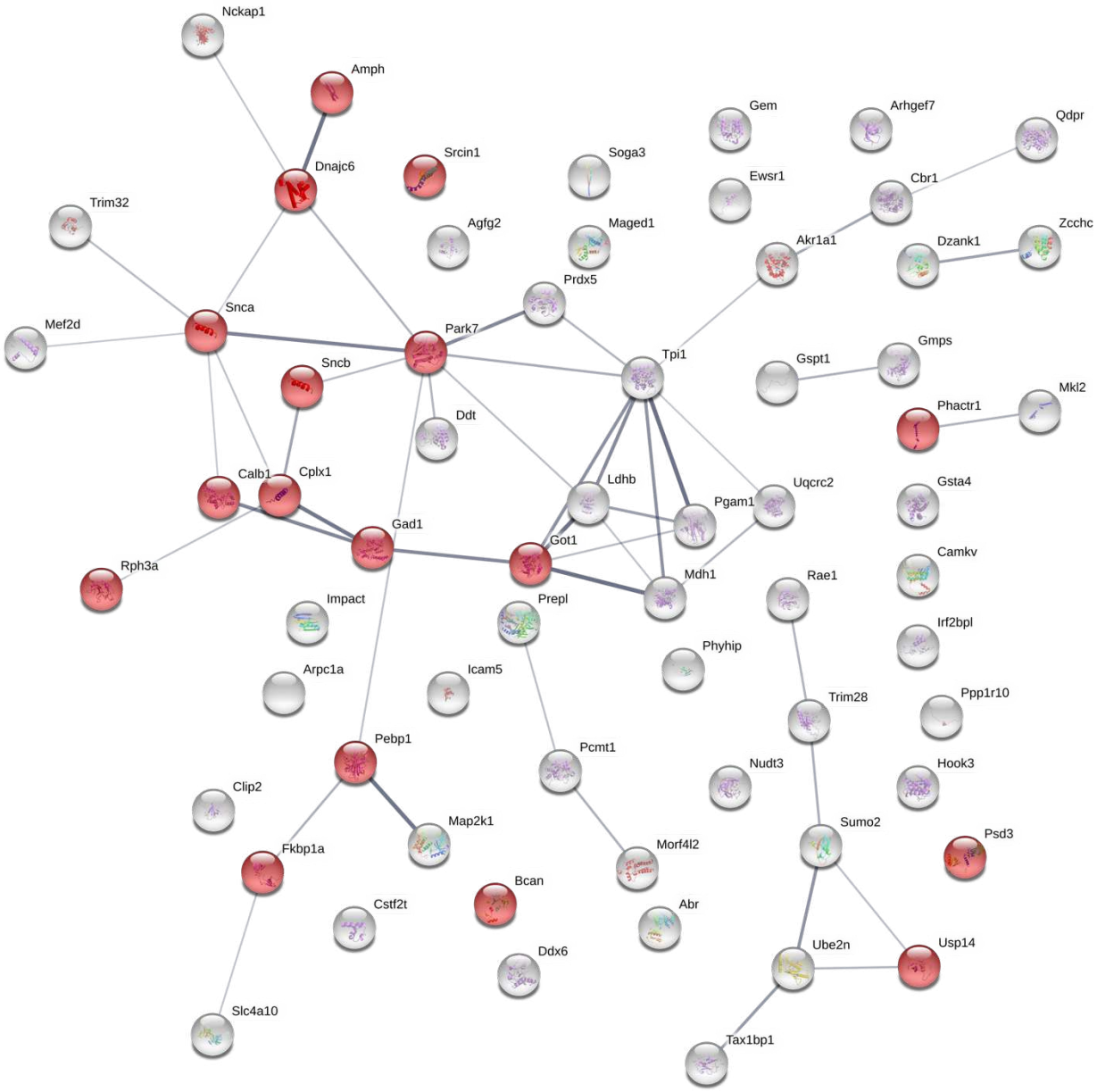

Supplementary Figure 6. Visual depiction of proteins in Hierarchical Cluster 2 (from Figure 5). String diagram showing biological networks between the proteins identified in Cluster 2. Figure generated by StringDb; Red node = GO: Synapse; FDR:5.6E-7.

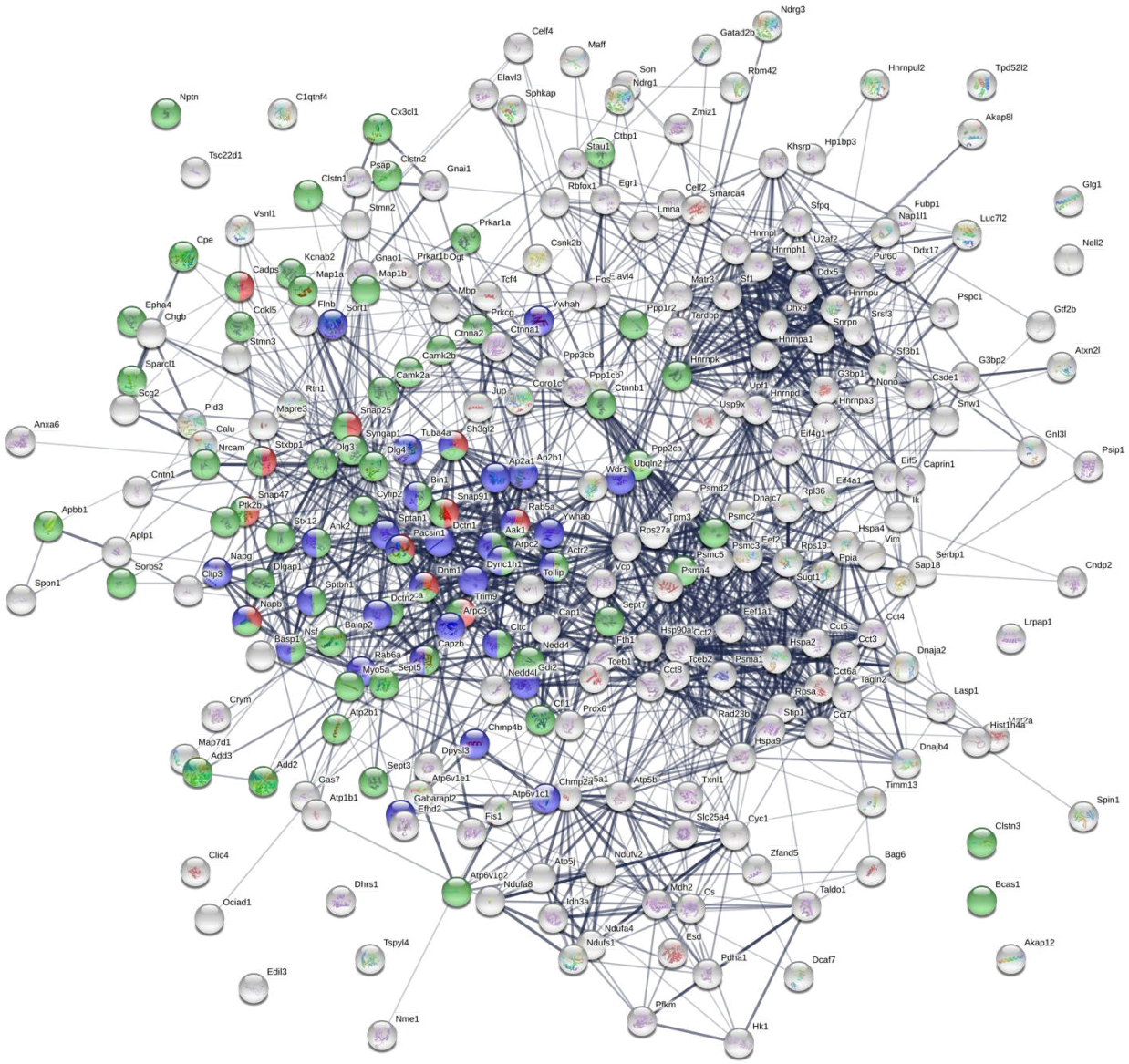

Supplementary Figure 7. Visual depiction of proteins in Hierarchical Cluster 3 (from Figure 5). String diagram showing biological networks between the proteins identified in Cluster 3. Figure generated by StringDb; Red node = GO: synaptic vesicle cycle (FDR: 2.77E-6); Green node = GO: synapse (FDR: 4.82E-29); Blue node = GO: membrane trafficking (FDR: 6.24E-11).

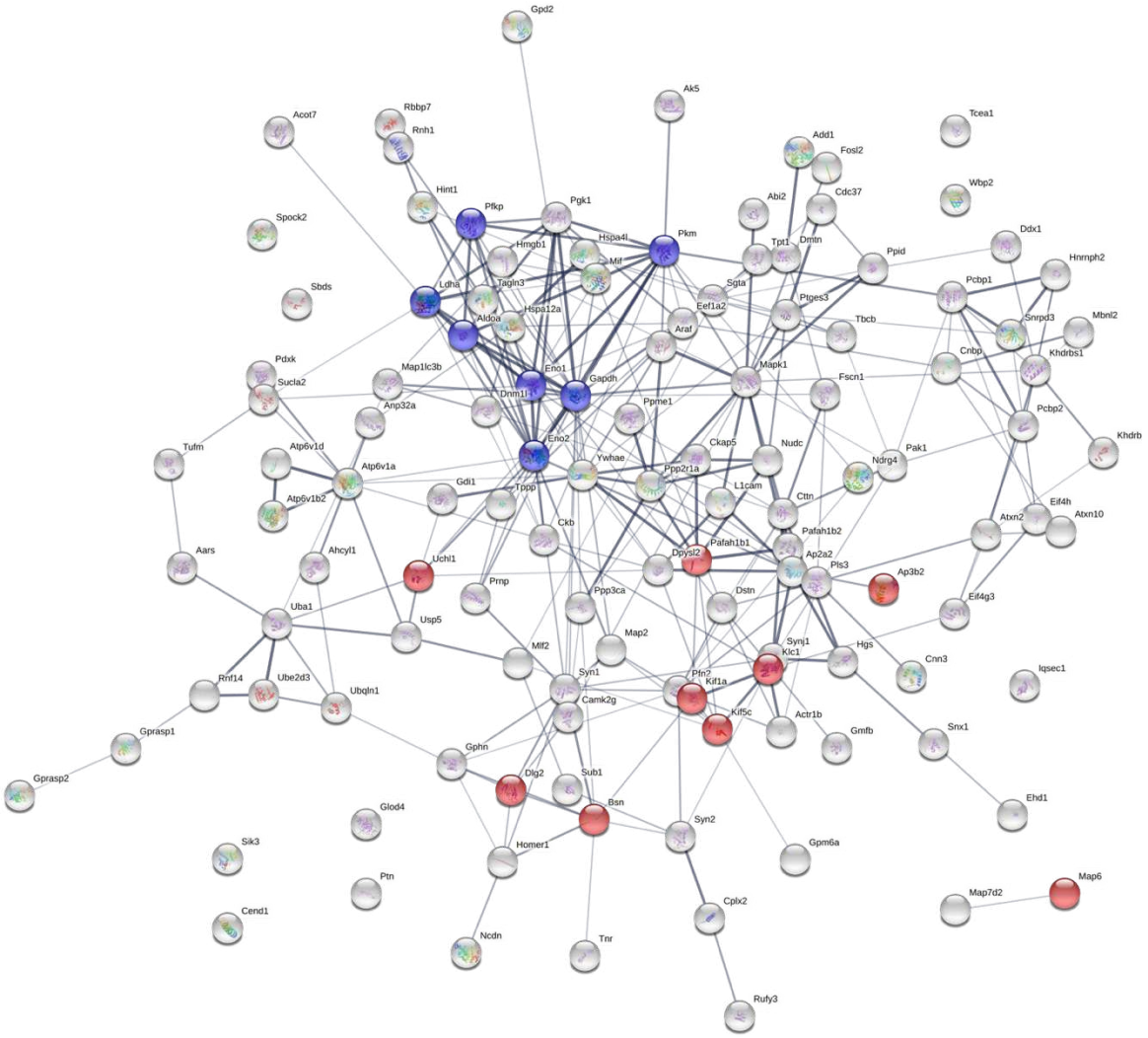

Supplementary Figure 8. Visual depiction of proteins in Hierarchical Cluster 4 (from Figure 5). String diagram showing biological networks between the proteins identified in Cluster 4. Figure generated by StringDb; Red node = GO: Axo-dendritic transport (FDR: 4.86E-8); Blue = GO: Glycolysis/Gluconeogenesis (FDR: 2.56E-5).

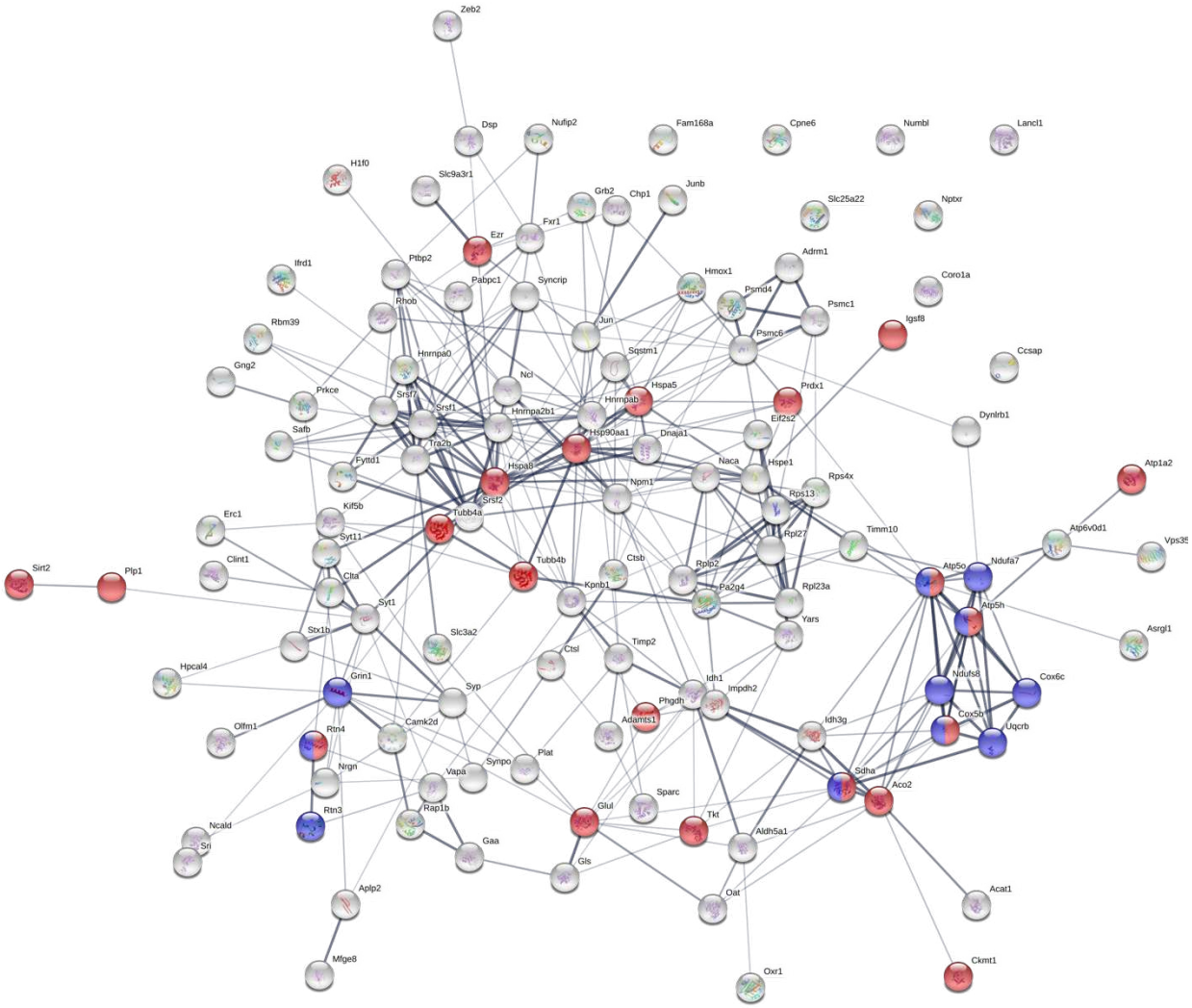

Supplementary Figure 9. Visual depiction of proteins in Hierarchical Cluster 5 (from Figure 5). String diagram showing biological networks between the proteins identified in Cluster 5. Figure generated by StringDb; Red node = GO: myelin sheath (FDR: 5.17E-18); blue node = GO: Alzheimer's disease (FDR: 8.16E-07).

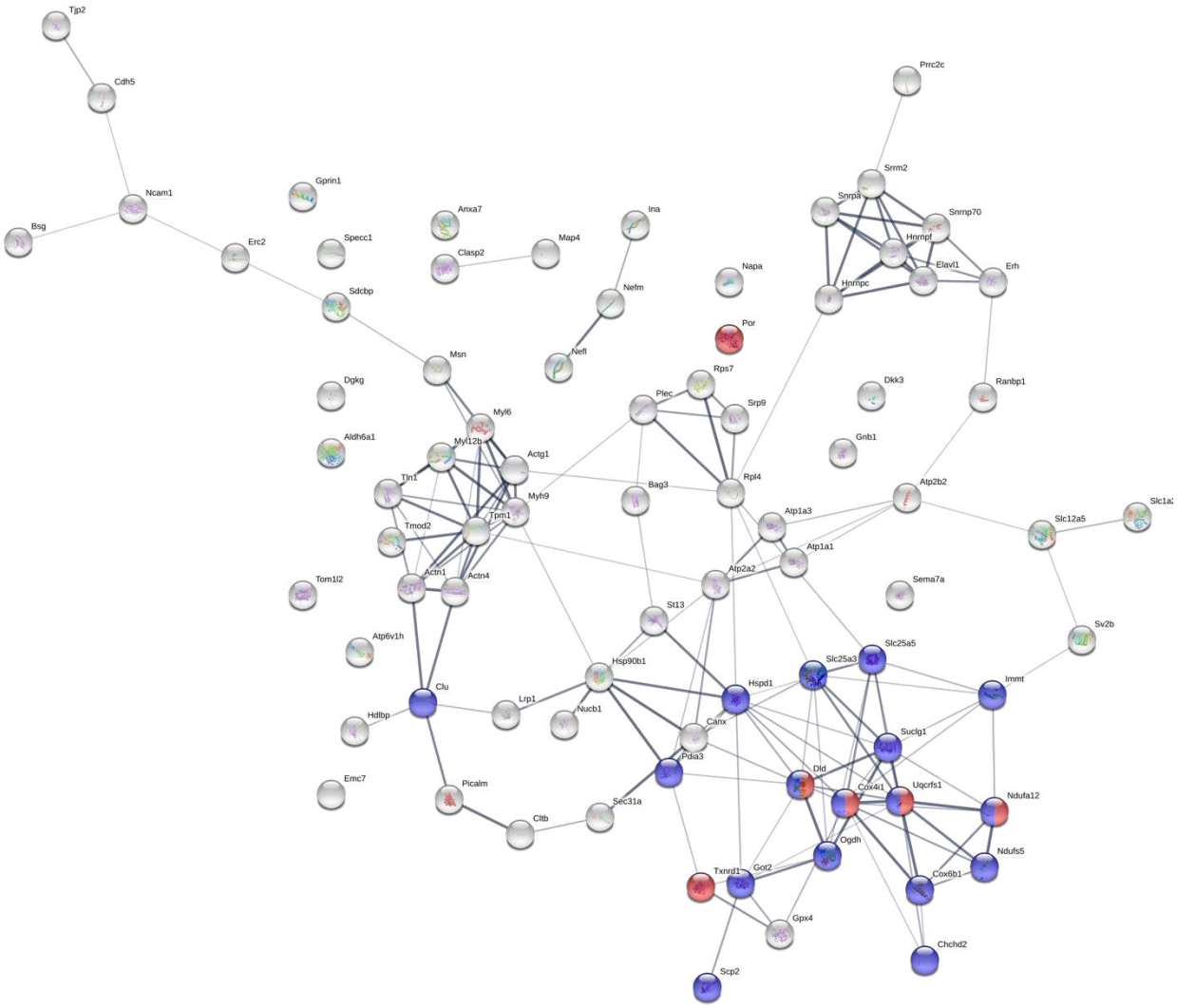

Supplementary Figure 10. Visual depiction of proteins in Hierarchical Cluster 6 (from Figure 5). String diagram showing biological networks between the proteins identified in Cluster 6. Figure generated by StringDb; Blue node = GO: mitochondrial part (FDR: 4.22E-07); Red node = GO: electron transfer activity (FDR: 2.88E-05).

Supplementary Table

Cluster 1	Cluster 2		Cluster 3									Cluster 4				Cluster 5			
Cat	Dzank1	Sumo2	Rab6a	Khsrp	Psap	Pdha1	Matr3	Dnaja2	Timm13	Cct7	Ank2	Aars	Dstn	Ldha	Rnh1	Ckmt1	Olfm1	Tubb4a	Yars
Plek	Sncb	Ube2n	Ppp1cb	Dnajb4	Camk2b	Sf3b1	Ctbp1	Fth1	Zmiz1	Ubqln2	Celf2	Abi2	Eef1a2	Map1lc3b	Rufy3	Kpnb1	Grin1	Psmd4	Gaa
Dpysl5	Fkbp1a	Prepl	Sept7	Cadps	Nell2	Dnajc7	Cct6a	Zfand5	Akap12	U2af2	Puf60	Acot7	Ehd1	Map2	Sbds	Fxr1	Timm10	Aplp2	Stx1b
Dnajb1	Ewsr1	Srcin1	Spin1	Idh3a	Cct4	Ap2a1	Dhx9	Stau1	Hk1	Kcnab2	Sparcl1	Actr1b	Eif4g3	Map6	Sgta	Ifrd1	Ptbp2	Sirt2	Camk2d
Vcam1	Tax1bp1	Dnajc6	Sf1	Tcf4	Hspa9	Chmp4b	Gatad2b	Rpl36	Glg1	Ndufa8	Ndrg1	Add1	Eif4h	Map7d2	Sik3	Pabpc1	Dnaja1	Cpne6	Atp5h
Atp1b2	Phactr1	Uqcrc2	Camk2a	Mat2a	Tceb2	Hp1bp3	Pld3	Eif4g1	Elavl4	Hnrnpd	Sept3	Ahcyl1	Eno1	Mapk1	Snrpd3	Hmox1	Mfge8	Ndufs8	Jun
Nfasc	Gsta4	Gmps	Fos	Nsf	Ppp2ca	Hsp90ab1	Napb	Dctn1	Maff	Arpc2	G3bp1	Ak5	Eno2	Mbnl2	Snx1	Ctsb	Coro1a	Hspe1	Syt11
Slc25a12	Amph	Trim32	Dlgap1	Ndufv2	Sept5	Tollip	Efhd2	Atp5a1	Myo5a	Celf4	Srsf3	Aldoa	Fosl2	Mif	Spock2	Hnrnpa0	Rps4x	Npm1	Clta
Ctsd	Arhgef7	Pcmt1	Luc7l2	Trim9	Sptbn1	Nptn	Basp1	Stmn2	Upf1	Dpysl3	Hnrnpa1	Anp32a	Fscn1	Mlf2	Sub1	Atp6v0d1	Plp1	Numbl	Hnrnpab
Ctss	Nckap1	Cplx1	Dync1h1	C1qtnf4	Calu	Gnao1	Cap1	Cfl1	Rtn1	Atp6v1c1	Taldo1	Ap2a2	Gapdh	Ncdn	Sucla2	Chp1	Plat	Erc1	Clint1
Srsf4	Soga3	Mef2d	Edil3	Gnl3l	Hnrnpk	Clic4	Ndrg3	Psma4	Eef2	Rbfox1	Psmc2	Ap3b2	Gdi1	Ndrg4	Syn1	Cox6c	Vps35	Impdh2	Rbm39
B2m	Ddt	Zcchc18	Psmd2	Snrpn	Serbp1	Ddx5	Dlg4	Napg	Txnl1	Nrcam		Araf	Glod4	Nudc	Syn2	Hspa8	Acat1	Cox5b	Dynlrb1
Ap2m1	Rph3a	Map2k1	Ctnna2	G3bp2	Csde1	Actr2	Nedd4l	Pfkm	Esd	Stxbp1		Atp6v1a	Gmfb	Pafah1b1	Synj1	Timp2	Fam168a	Rplp2	Oxr1
Pdia6	Tpi1	Arpc1a	Aplp1	Egr1	Prkar1b	Hspa4	Cdkl5	Nme1	Prkcg	Aak1		Atp6v1b2	Gpd2	Pafah1b2	Tagln3	Sparc	Ndufa7	Oat	Lancl1
Hyou1	Trim28	Morf4l2	Psip1	Nap1l1	Dctn2	Clip3	Rps27a	Akap8l	Gdi2	Hnrnpu		Atp6v1d	Gphn	Pak1	Tbcb	Slc25a22	Aldh5a1	Atp1a2	Hnrnpa2b1
Rpl8	Phyhip	Irf2bpl	Sfpq	Apbb1	Ogt	Eif5	Dhrs1	Cct5	Pspc1	Stmn3		Atxn10	Gpm6a	Pcbp1	Tcea1	Slc9a3r1	Igsf8	Glul	Gls
Aldh2	Mkl2	Maged1	Cct3	Fis1	Coro1c	Crym	Rps19	Eef1a1	Ppia	Atp6v1e1		Atxn2	Gprasp1	Pcbp2	Tnr	Grb2	Tubb4b	Ncald	Ccsap
Rbm3	Akr1a1	Icam5	Lrpap1	Cyfip2	Sh3gl2	Map7d1	Hnrnph1	Ndufs1	Cltc	Ik		Bsn	Gprasp2	Pdxk	Tppp	Psmc1	Adrm1	Naca	Prdx1
Apoe	Snca	Hook3	Tceb1	Hnrnpl	Cntn1	Lasp1	Atp5b	Sorbs2	Tagln2	Cndp2		Camk2g	Hgs	Pfkp	Tpt1	Ctsl	Hpcal4	Srsf2	Dsp
Anxa5	Impact	Cbr1	Add2	Hpca	Mapre3	Capzb	Ywhab	Atp5j	Fubp1	Mbp		Cdc37	Hint1	Pfn2	Tufm	Uqcrb	Asrgl1	Rpl27	Sri
Arglu1	Abr	Camkv	Tardbp	Smarca4	Tsc22d1	Psmc5	Sugt1	Atp2b1	Mdh2	Chmp2a		Cend1	Hmgb1	Pgk1	Uba1	Sdha	Idh3g	Hsp90aa1	Srsf1
Hsph1	Qdpr	Bcan	Cnp	Atxn2l	Psma1	Tpd52l2	Dlg3	Atp6v1g2	Gas7	Ppp3cb		Ckap5	Hnrnph2	Pkm	Ube2d3	Psmc6	Ezr	Safb	Tra2b
Adamts4	Agfg2	Calb1	Csnk2b	Clstn1	Arpc3	Flnb	Spon1	Ptk2b	Psmc3	Baiap2		Ckb	Homer1	Pls3	Ubqln1	Tkt	Syncrip	Prkce	Gng2
Pdhb	Prdx5	Mdh1	Ap2b1	Vsnl1	Ddx17	Rab5a	Sphkap	Gabarapl2	Vcp	Stx12		Cnbp	Hspa12a	Ppid	Uchl1	Nptxr	Junb	Synpo	Rps13
Ndufv1	Gem	Park7	Sort1	Epha4	Prdx6	Add3	Son	Elavl3	Usp9x	Slc25a4		Cnn3	Hspa4l	Ppme1	Usp5	Aco2	Phgdh	Idh1	Slc3a2
Sarnp	Pgam1	Psd3	Ctnna1	Cpe	Sptan1	Dnm1	Map1a	Lmna	Sept7	Tuba4a		Cplx2	Iqsec1	Ppp2r1a	Wbp2	Fyttd1	Rtn3	Eif2s2	H1f0
Anxa2	Nudt3	Pebp1	Ctnnb1	Clstn3	Pacsin1	Hspa2	Prkar1a	Gtf2b	Tspyl4	Chgb		Cttn	Khdrbs1	Ppp3ca	Ywhae	Adamts1	Rap1b	Hspa5	
Cand1	Ddx6	Gad1	Stip1	Jup	Hnrnpul2	Cct8	Ndufa4	Snap91	Bin1	Cyc1		Ddx1	Khdrbs3	Prnp		Atp5o	Rhob	Nufip2	
Stub1	Gspt1	Got1	Nedd4	Ppp1r2	Snap47	Rpsa	Syngap1	Atp1b1	Clstn2	Bcas1		Dlg2	Kif1a	Ptges3		Vapa	Syp	Rpl23a	
Col1a2	Usp14	Ldhb	Scg2	Nono	Rbm42	Anxa6	Cct2	Ywhah	Caprin1	Sap18		Dmtn	Kif5c	Ptn		Kif5b	Zeb2	Sqstm1	
Uqcrc1	Slc4a10	Ppp1r10	Bag6	Cs	Vim	Snw1	Snap25	Gnai1	Wdr1	Ociad1		Dnm1l	Klc1	Rbbp7		Pa2g4	Nrgn	Rtn4	
Rpl29	Clip2	Cstf2t	Tpm3	Hist1h4a	Map1b	Rad23b	Cx3cl1	Dcaf7	Hnrnpa3	Eif4a1		Dpysl2	L1cam	Rnf14		Ncl	Srsf7	Syt1	
PPI enrichment p-value:	**PPI enrichment p-value:**		**PPI enrichment p-value:**									**PPI enrichment p-value:**				**PPI enrichment p-value:**			
6.68E-05	**6.34E-09**		**< 1.0e-16**									**< 1.0e-16**				**< 1.0e-16**			
GO: protein processing in ER	**GO: synapse**		**Go: synaptic vesicle cycle**			**GO: membrane trafficking**			**GO: synapse**			**GO: glycolysis and gluconeogenesis**				**GO: myelin sheath**		**GO: Alzheimer's disease**	
FDR: 3.2E-4	**FDR: 5.6E-7**		**FDR: 2.77E-6**			**FDR: 6.24E-11**			**FDR: 4.82E-29**			**FDR: 3.02E-5**				**FDR: 5.17e-18**		**FDR:8.16e-07**	

Supplementary Table 1. Protein identities contained within key biological pathways as detected by the hierarchical clustering depicted in **Figure 5** and **Supplementary Figures 5-10.** BONLAC-detected proteins observed in both young and aged APP/PS1 and wild-type mouse hippocampus (n = 5-7 mice/genotype/group). PPI and FDR as detected via Cytoscape and StringDb.

Figures

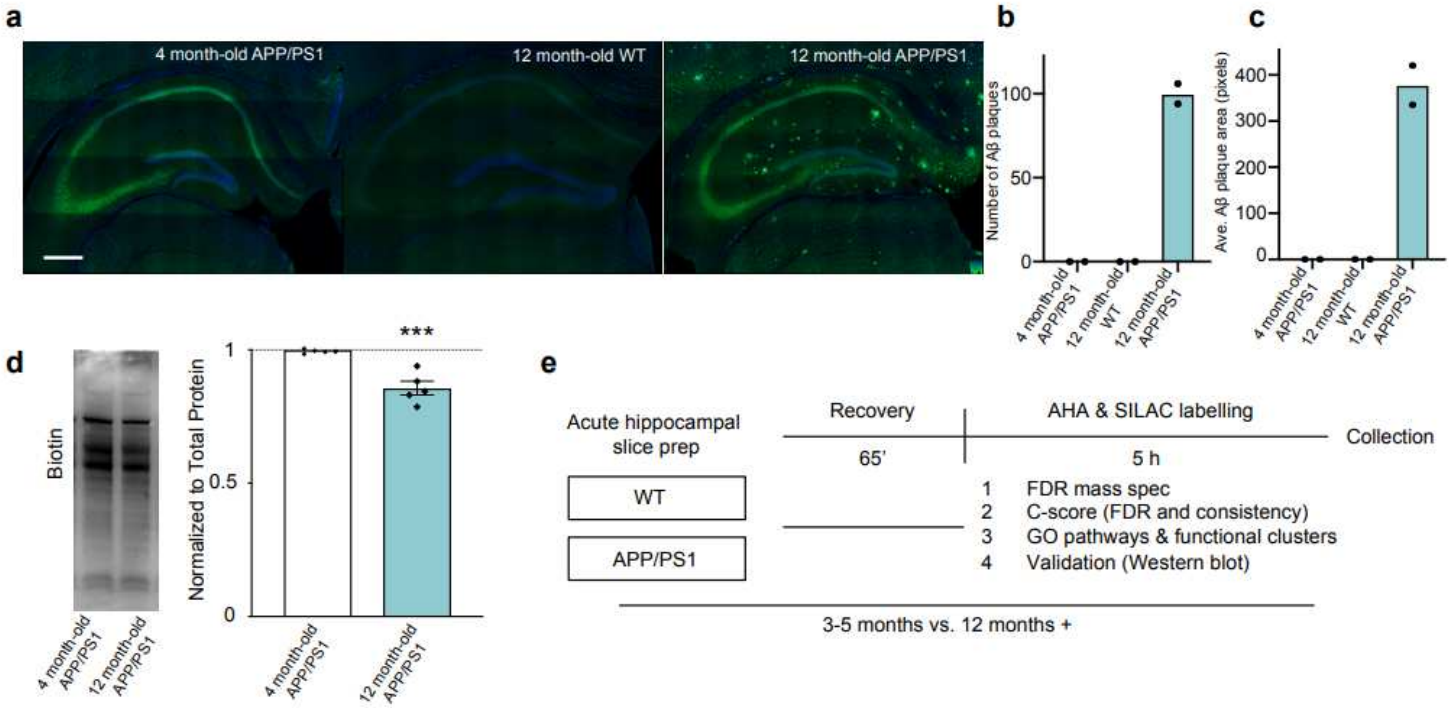

Figure 1

BONLAC-mediated labelling of de novo protein synthesis in the hippocampus of young and aged wild-type and APP/PS1 mice. a) Representative immunofluorescent images showing the progressive deposition of amyloid beta plaques in the hippocampus of 12 month-old APP/PS1 mice, but not 4 month-old APP/PS1 or 12 month-old wild-type (WT) mice (Blue = DAPI, Green = Aβ; scale bar = 50 μm). b) Quantification of the number of Aβ plaques in the hippocampus of 4 month-old APP/PS1 mice, 12 month-old WT and 12 month-old APP/PS1 mice. c) Quantification of the average area of the Aβ plaques observed in these groups (n = 1-2 mice per group for b and c). d) De novo synthesized protein in 3-5 month819 old vs. 12+ month-old APP/PS1 mouse hippocampal slices as detected via AHA labelling, followed by biotin-alkyne click reaction and western blot (normalized to total protein (as determined via MemCode staining), expressed relative to average 4 month-old biotin signal; n = 5 mice/condition; error bars show mean ± SEM, statistical significance calculated using unpaired two tailed t test: t = 5.545, 95% confidence interval = -0.02033 to -0.08388, effect size = -0.1436 ± 0.0259, df = 8, p = 0.0005). e) Schematic showing BONLAC workflow for acute hippocampal slices from WT and APP/PS1 mice. Following labelling, slices from one APP/PS1 and one age-matched WT mouse are pooled for subsequent processing.

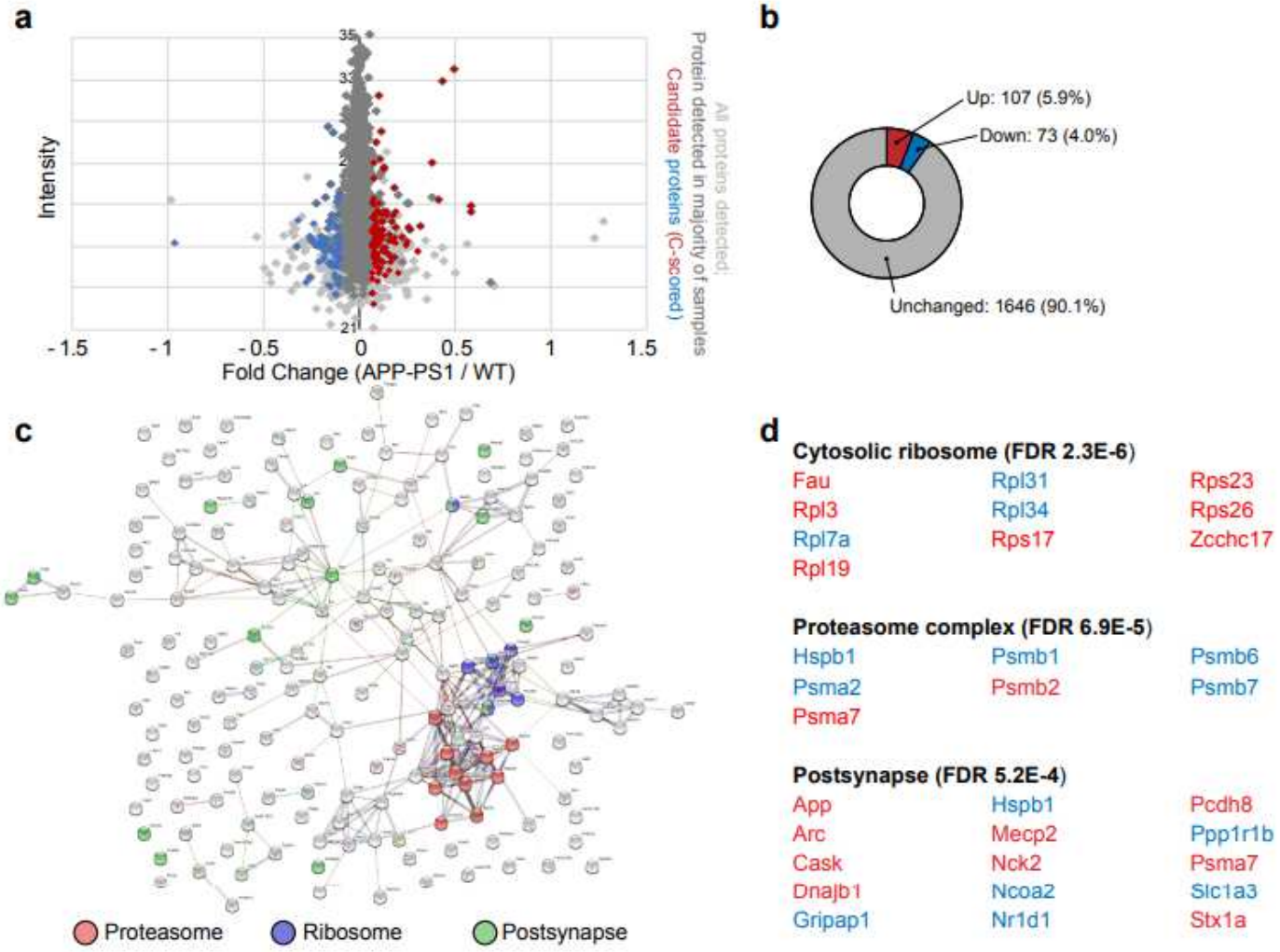

Figure 2

Steady state proteome differs in young wild-type and APP/PS1 mouse hippocampus. a) Fold change vs. intensity distribution plot of all newly made proteins detected in wild-type (WT) vs. 3-5 month-old APP/PS1 hippocampus (light grey), with proteins that were detected in majority of samples (>3 out of 5 samples; grey) and dysregulated candidate proteins identified by C-score screen (upregulated ≥ 20% in red, downregulated ≤ 20% in blue). b) Doughnut plot showing the proportion of detected proteins that were downregulated (fold change < 0.8, blue), upregulated (fold change > 1.2, red) or unchanged in the majority of 4 month-old APP/PS1 mice compared to WT littermates. c) String diagram depicting enriched gene ontology groups. d) Top functional clusters in 3-5 month-old APP/PS1 mice compared to WT using DAVID. Red = upregulated proteins. Blue = downregulated proteins.

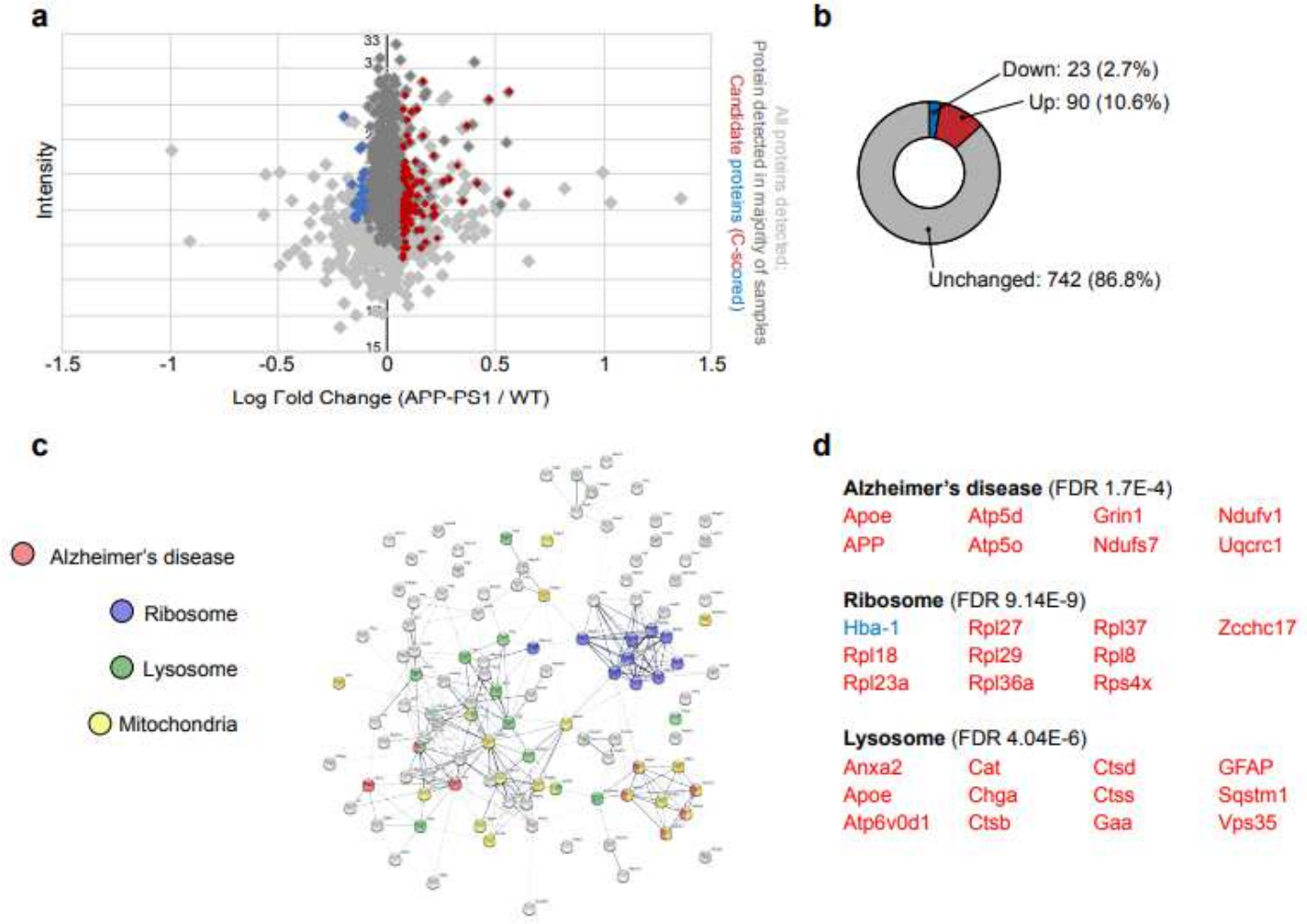

Figure 3

Analysis of altered de novo proteome highlights impaired proteostasis in aged APP/PS1 mice. a) Fold change vs. intensity distribution plot showing all proteins detected in 12+ month-old APP/PS1 mouse hippocampal slices vs. wild-type (WT) littermates using BONLAC (light grey). Dark grey overlay depicts proteins that were consistently detected in the majority of samples (>4/7), and candidate proteins identified by C-score screen as upregulated (fold change ≥ 1.2) shown in red, while downregulated proteins (≤ 0.8) are labelled blue. b) Doughnut plot indicating the majority of proteins detected in 12+ month-old mice are not altered in APP/PS1 mice (742; 86.8% of proteins detected). 23 proteins are downregulated compared to WT mice (2.7% of proteins show a fold change >0.8, blue) and 90 proteins are upregulated in APP/PS1 mice (10.6% of proteins show a fold change <1.2, red). c) String diagram showing enriched gene ontology networks. d) DAVID-identified functional clusters in 12+ month-old APP/PS1 mice. Red =upregulated proteins. Blue = downregulated proteins.

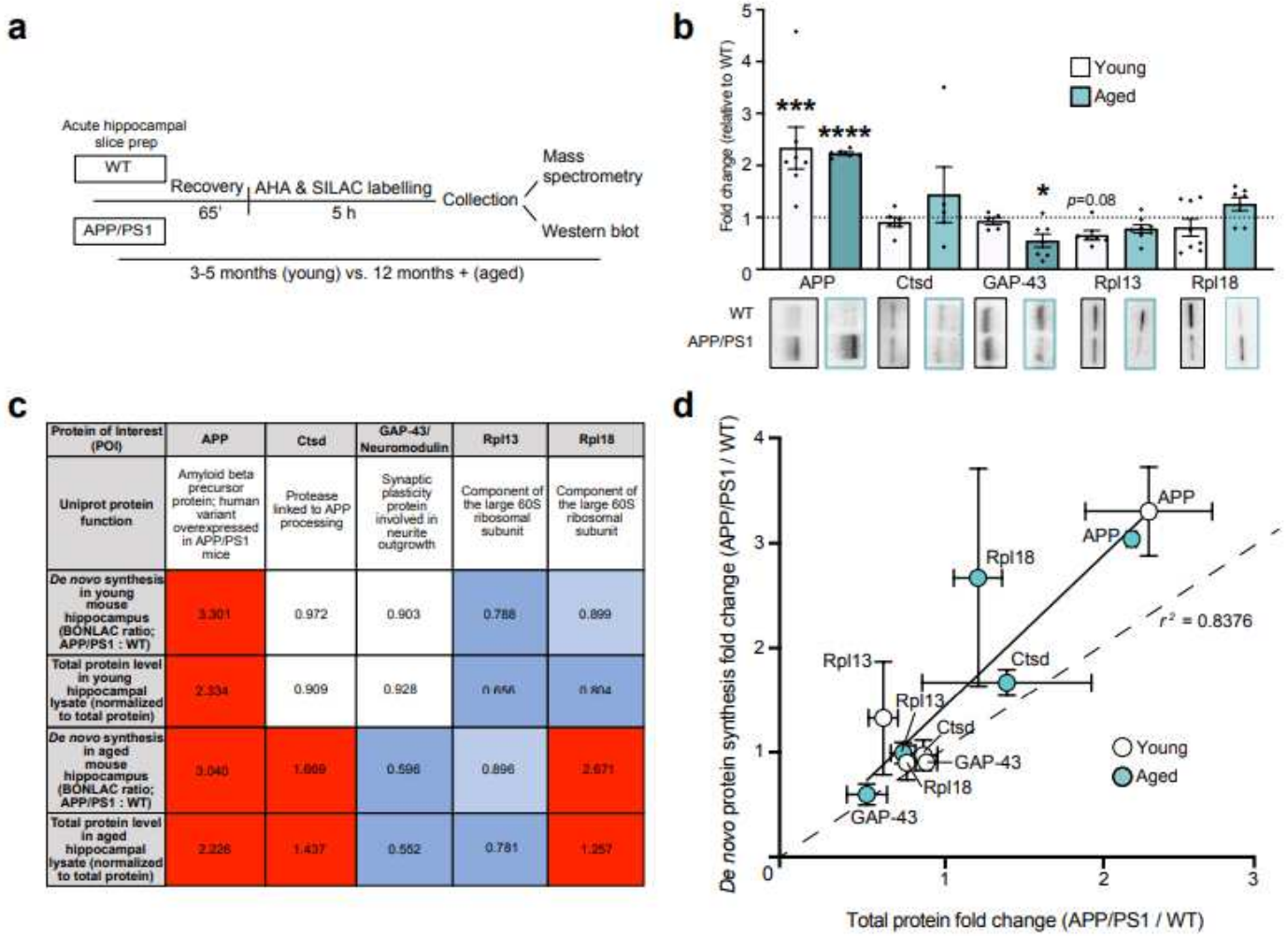

Protein of interest (POI)	APP	Ctsd	GAP-43/ Neuromodulin	Rpl13	Rpl18
Uniprot protein function	Amyloid beta precursor protein; human variant overexpressed in APP/PS1 mice	Protease linked to APP processing	Synaptic plasticity protein involved in neurite outgrowth	Component of the large 60S ribosomal subunit	Component of the large 60S ribosomal subunit
De novo synthesis in young mouse hippocampus (BONLAC ratio; APP/PS1 : WT)	3.301	0.972	0.903	0.788	0.899
Total protein level in young hippocampal lysate (normalized to total protein)	2.334	0.909	0.928	0.666	0.804
De novo synthesis in aged mouse hippocampus (BONLAC ratio; APP/PS1 : WT)	3.040	1.669	0.596	0.896	2.671
Total protein level in aged hippocampal lysate (normalized to total protein)	2.226	1.437	0.552	0.781	1.257

Figure 4

Candidate proteins identified with BONLAC screen of de novo proteome exhibit altered expression levels in APP/PS1 mice. a) Schematic of workflow for slice allocation for mass spectrometry and western blot protein validation. b) Western blot quantitation of candidate proteins selected from BONLAC screen in 3-5 month-old (young; white bars) and 12+ month-old (aged; teal bars) mice, normalized to total protein (as assessed by MemCode) and expressed relative to wild-type (WT; n = 5-8 mice; error bars show mean ± SEM; statistical significance calculated between APP/PS1 and WT samples using unpaired two tailed t tests; young APP: t = 4.117, 95% confidence interval = 0.6495 to 2.028, effect size = 1.339 ± 0.3252, df = 16, p = 0.0008; aged APP: t = 15.29, 95% confidence interval =1.046 to 1.402, effect size = 1.224 ± 0.08007, df = 10, p < 0.0001; aged GAP-43: t = 2.266, 95% confidence interval = -0.9047 to -0.01774, effect size = -0.4612 ± 0.2035, df = 12, p = 0.0427; young Rpl13: t = 2.004, 95% confidence interval = -0.9413 to 0.07764, effect size = -0.4318 ± 0.2154, df = 7, p = 0.0851).; representative western blots showing selected protein levels in WT and APP/PS1 mouse hippocampal lysates (young: black box; aged: teal box). c) Comparison table showing average fold change in de novo synthesis of candidate proteins in young and aged APP/PS1 vs WT littermates as identified by BONLAC (young n=5; aged n=7) compared to change in total expression quantified by western blot. Vibrant color indicates value reached cutoff (+/-

20%; >0.8 or < 1.2); pale color indicates near threshold (within 5%); white indicates no change. d) Simple linear regression showing correlation between average de novo synthesized protein fold-change (as determined by BONLAC) vs. average total protein fold-change (as determined via western blot) of candidate proteins in the APP/PS1 vs. WT hippocampus at 3-5 months (white circles) and 12+ months of age (teal circles; figure shows mean ± SEM (vertical error bars: BONLAC; horizontal error bars: western blot); r 2 value = 0.8376, F = 41.25, DFn, DFd = 1, 8, p = 0.0002).

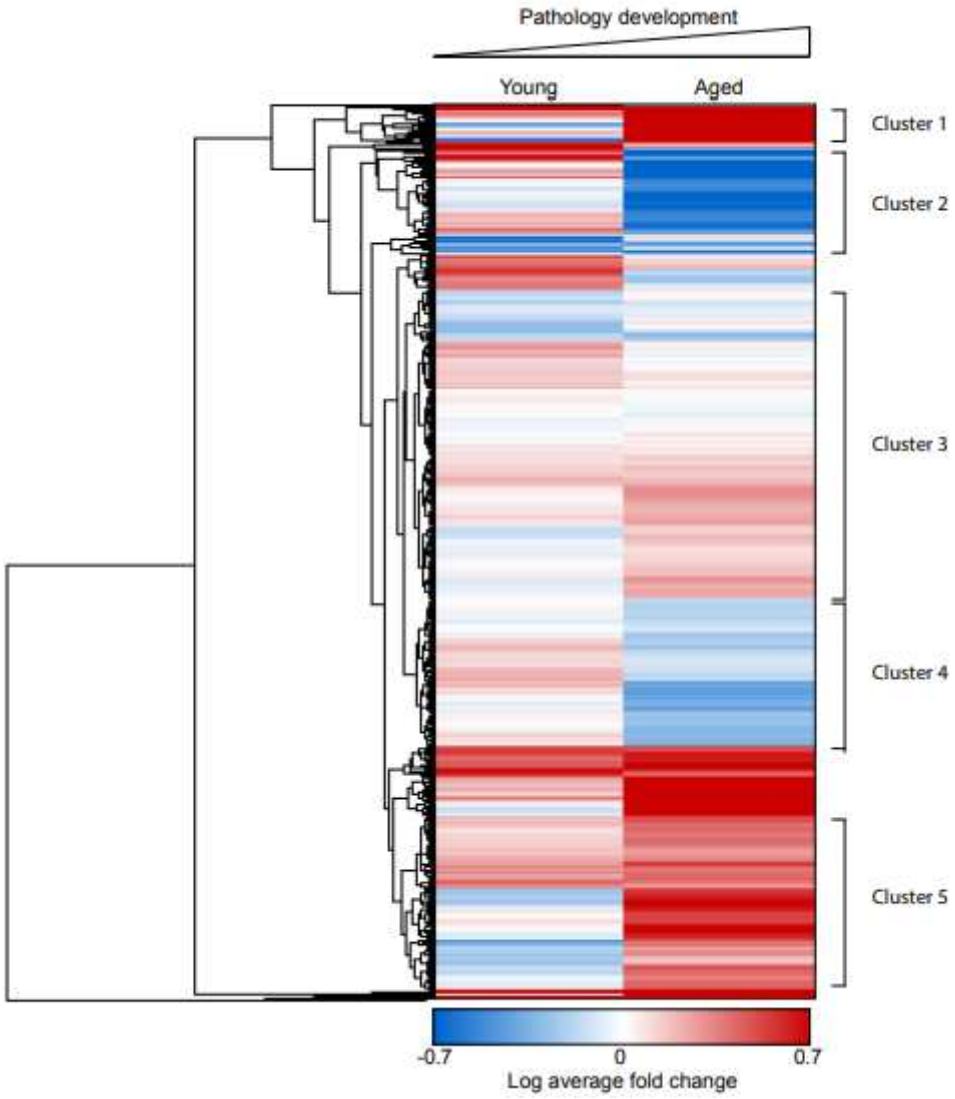

Figure 5

The biological pathways affected by dysregulated hippocampal protein synthesis vary with age in APP/PS1 mice. Hierarchical clustering heatmap reveals similarities and divergence in the mean-normalized log protein fold change of the 791 proteins detected in both young (3-5 months-old) and aged (12+ months-old) APP/PS1 mice relative to wild-type (WT) littermates. GO analysis evidenced 6 major clusters being significantly modified, which are: 1) protein processing in the endoplasmic reticulum (FDR 3.2E-04); 2) synapse (FDR 5.6E-07); 3) synaptic vesicle cycle (FDR 2.77E-06), membrane trafficking (FDR 6.24E-11) and synapse (FDR 4.82E-29); 4) axo-dendritic transport (FDR 4.86E-08) and

glycolysis/gluconeogenesis (2.56E-05); 5) myelin sheath (5.17E-18) and Alzheimer's disease (8.16E-07); and 6) mitochondrial part (FDR 2.54E-08) and electron transfer activity (FDR 4.02E-05). FDR generated by StringDB algorithms. Red = upregulated proteins. Blue = downregulated proteins. White = unchanged protein expression.

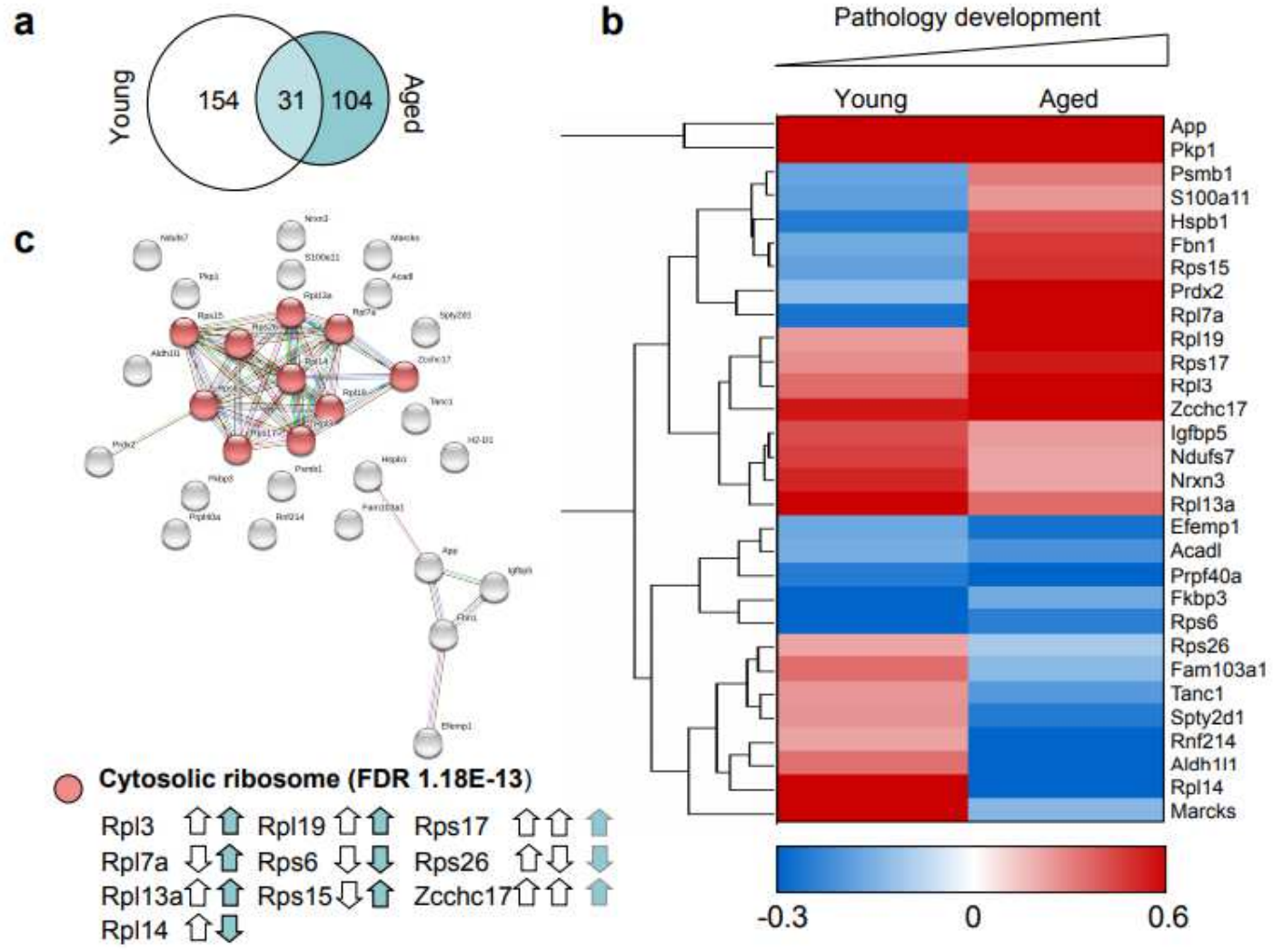

Figure 6

Steady state proteome is predominantly distinct throughout aging. a) Minimal overlap is observed between proteins that are dysregulated (as detected by C-score rank algorithm) in the hippocampi of 3-5 month-old (young) vs. 12+ month-old (aged) APP/PS1 mice. b) Hierarchical clustering of log fold changes reveals the majority of proteins which are dysregulated in both young and aged APP/PS1 mice compared to WT littermates do not show the same trend. Red = upregulated proteins. Blue = downregulated proteins. White = unchanged protein expression. c) String diagram revealing an enrichment of proteins in the GO network 'Cytosolic ribosome' in APP/PS1 throughout the aging process. White arrows = direction of regulation in young mice. Teal arrows = direction of regulation in aged mice

Supplementary Files

This is a list of supplementary files associated with this preprint. Click to download.

- Elder.et.alSupplementarydata.xlsx